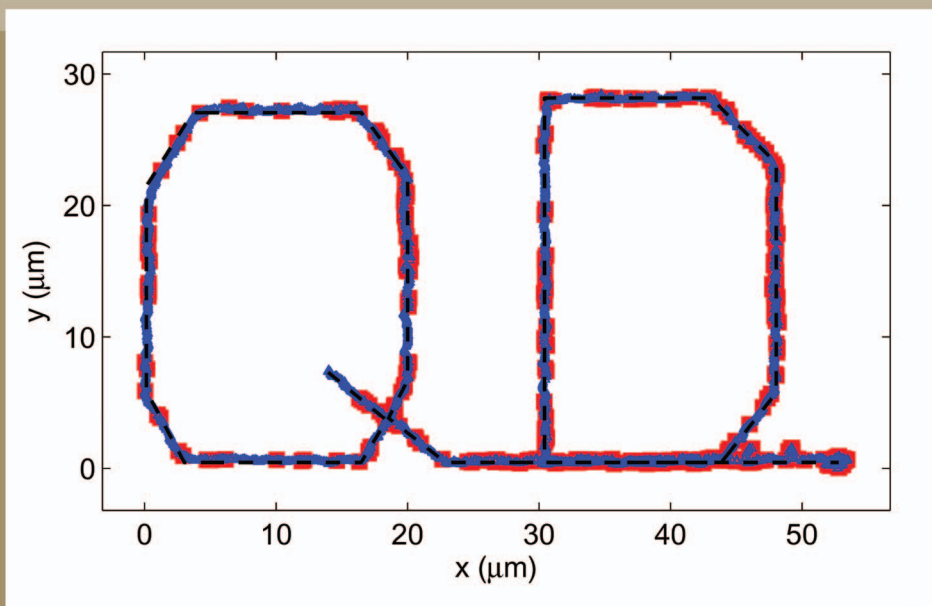
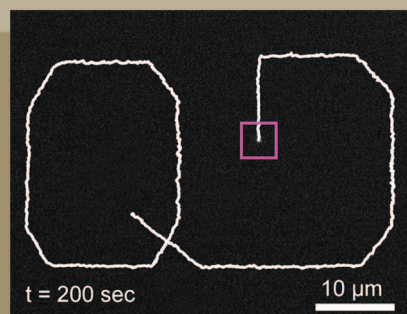
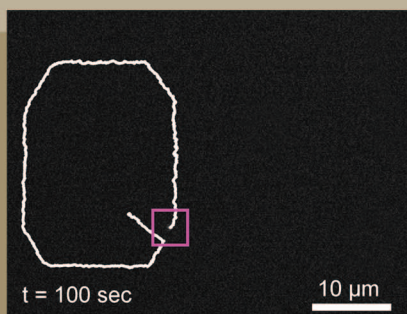
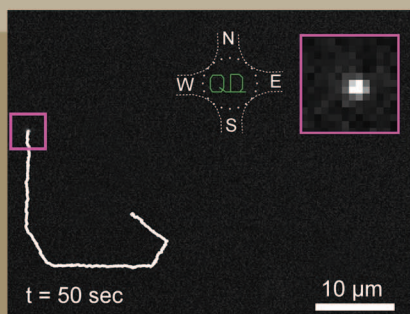


IEEE

control systems

MAGAZINE

APRIL 2012 VOLUME 32 NUMBER 2



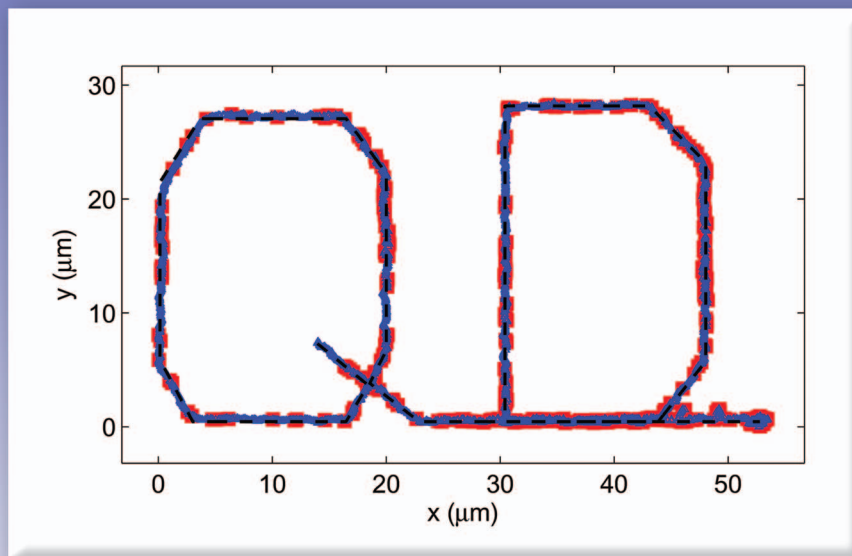
On-Chip Control



Control Systems Society
Advancing Control Science
and Technology



Flow Control of Small Objects on Chip



MANIPULATING LIVE CELLS, QUANTUM DOTS, AND NANOWIRES

This article is on microscale flow control, on dynamically shaping flow fields in microfluidic devices to precisely manipulate cells, quantum dots (QDs), and nanowires (Figure 1). Compared to prior methods (Table 1), manipulating microscopic and nanoscopic objects by flow control can be achieved with simpler and easy-to-fabricate devices, can steer a wider variety of objects, and enables entirely new capabilities such as placement and immobilization of specific quantum dots to desired on-chip locations with nanoscale precision. A companion article [267] investigates flow control in the body

ROLAND PROBST,
ZACHARY CUMMINS,
CHAD ROPP, EDO WAKS,
and BENJAMIN SHAPIRO

and develops methods to shape magnetic fields to direct ferrofluids of therapeutic magnetic nanoparticles to disease locations in patients.

Microfluidic systems have features (channels, valves, wells, posts, and chemically modified patches) that range in size from millimeters to micrometers [1], [2]. Nanofluidic devices usually refer to on-chip systems that contain nanoscopic features (nanoscale wires, junctions, or pores) [3], [4]. The size of micro/nanoscale actuators and sensors matches the size of biological entities (see “The Size of Things”). These entities include bacteria, plant, and animal cells ($\sim 1\text{--}100\ \mu\text{m}$ diameter), viruses ($\sim 10\text{--}100\ \text{nm}$), and DNA (2 nm wide but can be very long as a human cell contains about 1 m of DNA). As a result, microfluidic and nanofluidic devices

Modeling and feedback control has enabled simple PDMS on glass devices to manipulate a variety of cells including bacteria, animal cells, and live human cells to single micron precision.

have found applications in biology and medicine and have been used for rapid analysis of DNA, for analysis and detection of proteins, for monitoring and analysis of cells, and for implantable drug injection systems [5]–[9]. With DNA and proteins, the goal is often to amplify specific DNA sequences or separate out rare proteins from a background of common ones to enable sensitive detection of pathogens or diseases [10]–[13]. Live cells are monitored to answer basic-science biology questions (such as how do these cells interact one with another [14], [15]) or to better choose treatment options (such as which cancer drugs can kill this patient’s tumor cells most effectively [16], [17]). In microfluidic systems developed for such purposes, a need has emerged to more precisely and reliably manipulate biological entities and to steer elements (cells, DNA fragments, viruses, or proteins) to on-chip sensors and into biochemical reaction chambers. Feedback control can help; it enables the manipulation of particles and biomolecules with higher precision, faster, with increased throughput (more objects at once), and in messy biological environments with uncertain parameters and conditions.

Table 1 provides an overview of existing capabilities for manipulation of microscopic and nanoscopic objects. The first column summarizes the actuation physics. The left half of the second column lists which types of objects have been manipulated (see the symbol key in the table header) while the right half states to what accuracy; for example, in [28], cells were manipulated using handles with a translational accuracy of less than $1\ \mu\text{m}$ and an angular velocity accuracy quantified in degrees per second ($^\circ/\text{s}$). The third column describes the applied forces; at the top of each row, in bold, is stated how the forces scale with object size or charge; underneath, a force scale bar states the range of forces demonstrated in experiments. The fourth column summarizes the working distance of the method; at the top, in bold, is stated how forces scale with distance from the actuator or actuators, and below a typical distance range is stated. The fifth column notes if the method has or has not been able

to trap and steer multiple objects at once. Likewise, columns six and seven state if manipulation in three dimensions and control of object rotation has been achieved. Column eight summarizes typical hardware requirements and column nine notes if the manipulation technique typically includes feedback control.

Laser tweezers are the current gold standard for particle manipulation [18], [20], [30], [82]–[85]. In a classical optical tweezer system, when a dielectric particle is within the beam but off center, it deflects the laser light and the resulting change in light momentum exerts an equal and opposite force on the particle, which brings it back to the beam center [18], [30]. So long as the particle does not escape the laser beam, steering the beam steers the particle. Holographic laser tweezers can split one source beam into many individually controlled spots, and this has allowed steering of up to ~ 400 particles at once in all three dimensions [19], [26], [86], [87]. The size of controlled particles has ranged from 80-nm-diameter gold nanoparticles [24] to $50\ \mu\text{m}$ microorganisms [88], with applied forces ranging in magnitude from femto (10^{-15}) to piko (10^{-12}) Newtons [19], [30].

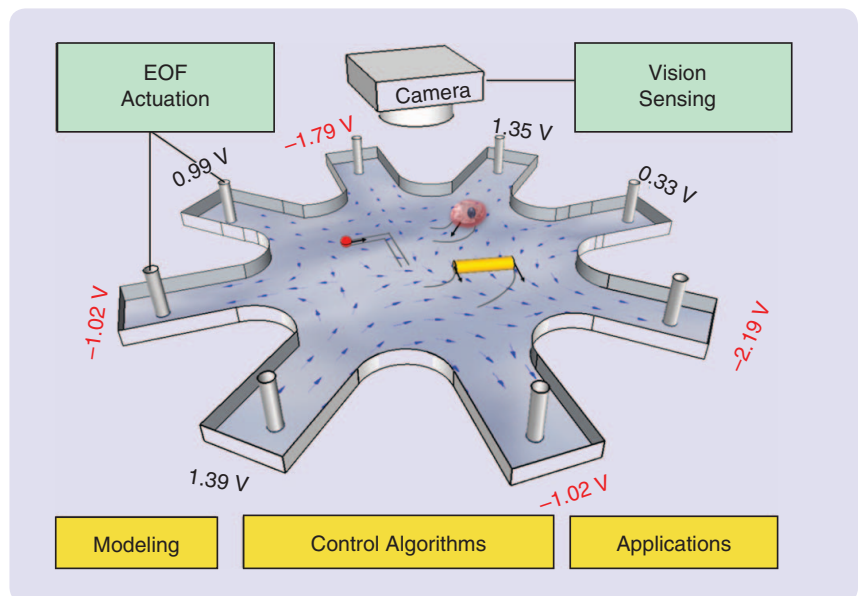


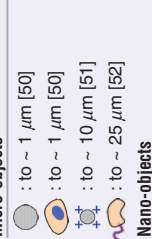

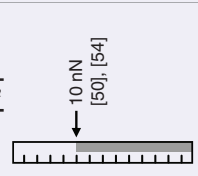
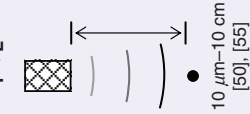





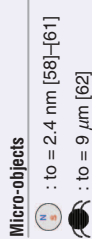


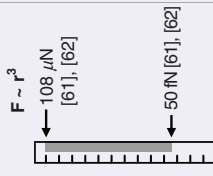
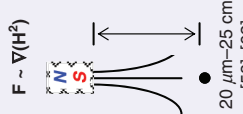
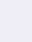
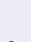


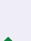
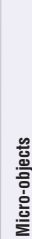

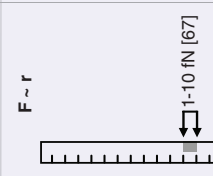
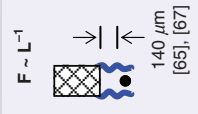

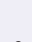



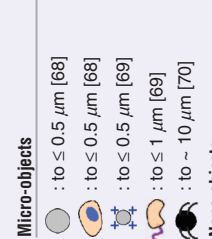
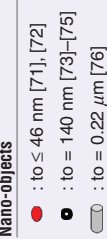
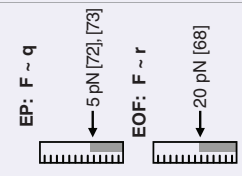
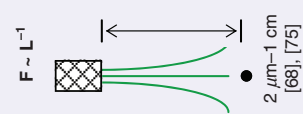
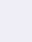
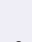


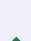
FIGURE 1 The goal is to control microflows to manipulate micro- and nanoscopic objects [quantum dots (QDs), cells, and nanowires] with high precision on chip. The image shows a controlled flow that is simultaneously transporting a QD (small red dot), a cell (pink sphere), and a wire to their desired positions (blue arrows show the flow, four black arrows highlight flow directions at four critical locations). This article discusses the electroosmotic flow actuation, vision sensing, modeling, control algorithms, experiments, and sample applications for this type of microscale flow control.

TABLE 1: Summary of particle control capabilities.

KEY: **F** Force **r** Object radius **l** Object length **L** Length from actuator

Bead
 Bead with surface charge
 Conducting bead
 Magnetic bead
 Fluorescent bead
 Quantum dot
 Nanorod
 Cell
 Swimming cell
 Bacterium
 Virus
 Molecule
 Microrobot
 Cell with bead
 Cell with magnetic bead
 DNA with bead

Actuation Physics	Have Controlled: To Accuracy	Forces: Scaling/Range	Actuation Distance: Scale/Range	Steer/Trap Multiple Particles?	In 3D?	Control Rotation?	Hardware	Got Feedback?
<p>Laser Tweezers</p> <p>Deflection of high intensity laser light lines up dielectric particle with the laser [18].</p>	<p>Micro-objects</p> <ul style="list-style-type: none"> : to ~ 1 μm [19] : to ~ 1 μm [20] : to < 1 μm [23], [24] <p>Nano-objects</p> <ul style="list-style-type: none"> : to < 40 nm [24], [25] : to < 1 μm, < 1° [26] : to < 1 μm [28] <p>Using particles as a handle</p> <ul style="list-style-type: none"> : to < 1 μm, 5.7°/s [28] : to = 20 nm [29] 	<p>$F \sim r^3$</p> <p>1 mN ← 100 pN [30] ← 0.2 fN [36] 0.01 fN</p>	<p>Long working distance (cm)</p>	<p>Trap? </p> <p>BioRyx, [19]</p> <p>Steer? </p> <p>BioRyx, [19]</p>	<p></p> <p>BioRyx, [19]</p>	<p></p> <p>[28], [31], [32]</p>	<p>Complex and expensive optical setups required to generate stable traps.</p>	<p>Optical trapping itself is passive, but xyz stages to move the sample usually operate with feedback</p>
<p>Dielectrophoretic</p> <p>Dielectric particle displaced in a spatially nonuniform dc and ac electric field (E).</p>	<p>Micro-objects</p> <ul style="list-style-type: none"> : to < 1 μm [33]–[36] : to < 1 μm [37] <p>Nano-objects</p> <ul style="list-style-type: none"> : to ~ 1 μm [38], [39] : to ~ 1 μm [38], [39] : to ~ 1 μm [40] 	<p>$F \sim r^3$</p> <p>50 pN [36] 25 pN [33] 0.7 pN [41] 76 fN [37]</p>	<p>$F \sim \nabla(E^2)$</p> <p>400 μm [37]</p>	<p>Trap? </p> <p>[33]</p> <p>Steer? </p>	<p></p>	<p></p> <p>[37]</p>	<p>2D and 3D microfabricated electrode structures and high frequency signal generators [1 kHz –20 MHz] to generate sufficient gradient forces.</p>	<p></p> <p>[37], with [42], [43] including advanced control algorithm design</p>
<p>Optoelectronic</p> <p>Particles dielectrophoretically manipulated by light-induced virtual electrodes that concentrate electric fields on the illuminated surface.</p>	<p>Micro-objects</p> <ul style="list-style-type: none"> : to 1 - 10 μm [44] : to 0.15 - 0.5 μm [45]–[47] <p>Nano-objects</p> <ul style="list-style-type: none"> : to ~ 1 μm [48] : to = 0.22 μm [49] 	<p>$F \sim r^3$</p> <p>14.5 pN [47] 0.1 pN [48]</p>	<p>$F \sim \nabla(E^2)$</p> <p>18 mm [44]</p>	<p>Trap? </p> <p>[44]</p> <p>Steer? </p>	<p></p>	<p></p>	<p>Substrates coated with a transparent conducting material, and a light source that can produce images [digital micro mirror device (DMD) or phototransistor substrate].</p>	<p></p> <p>[45]</p>

Acoustic	Actuation Physics	Have Controlled: With Accuracy	Forces: Scaling/Range	Actuation Distance: Scale/Range	Steer/Trap Multiple Particles?	In 3D?	Control Rotation?	Hardware	Got Feedback?
	Ultrasonic standing waves with associated pressure maxima and minima. Particles move to pressure nodes due to axial radiation forces.	Micro-objects  <ul style="list-style-type: none"> : to ~ 1 μm [50] : to ~ 1 μm [50] : to ~ 10 μm [51] : to ~ 25 μm [52] Nano-objects  <ul style="list-style-type: none"> : to ~ 1 μm [53] 	 <p>$F \sim r^3$ 10 nN [50], [54]</p>	<p>$F \sim L^{-3}$</p>  <p>10 μm–10 cm [50], [55]</p>	<p>Trap?  [56]</p> <p>Steer?  [57]</p>	 [53], [57]		Technique requires piezoelectric transducers, function generators, amplifiers, and a sample chamber.	
Magnetic	Attraction of magnetic particles by electromagnetic fields (H).	Micro-objects  <ul style="list-style-type: none"> : to = 2.4 nm [58]–[61] : to = 9 μm [62] Nano-objects  <ul style="list-style-type: none"> : to = 20 nm [58] Using particles as handle  <ul style="list-style-type: none"> : to = 8 μm [63] 	 <p>$F \sim r^3$ 108 μN [61], [62] 50 fN [61], [62]</p>	<p>$F \sim \nabla(H^2)$</p>  <p>20 μm–25 cm [58], [62]</p>	<p>Trap?  [63]</p> <p>Steer?  [63]</p>	 [62]	 [62]	Technique uses: customized electromagnets.	 [60]–[62], [64]
Hydrodynamic Trap	A fluid stagnation point is created by directing two laminar flows into a cross-slot junction. The stagnation point is a stable point (zero-velocity point) that is used to trap the particle [66].	Micro-objects  <ul style="list-style-type: none"> : to = 2.2 μm [65] Nano-objects  <ul style="list-style-type: none"> : to = 100 nm [65] 	 <p>$F \sim r$ 1–10 fN [67]</p>	<p>$F \sim L^{-1}$</p>  <p>140 μm [65], [67]</p>	<p>Trap? </p> <p>Steer? </p>			Technique uses: disposable microfluidic devices.	 [65], [66]
Electrokinetic Tweezers	Electrophoretically: An applied electric field creates an electrostatic force on objects with surface charge (q). Electroosmotically: Fluid flow is created by electrostatic forces acting on a thin layer of ions at fluid/device interfaces. This flow transports the objects.	Micro-objects  <ul style="list-style-type: none"> : to ≤ 0.5 μm [68] : to ≤ 0.5 μm [68] : to ≤ 0.5 μm [69] : to ≤ 1 μm [69] : to ~ 10 μm [70] Nano-objects  <ul style="list-style-type: none"> : to ≤ 46 nm [71], [72] : to = 140 nm [73]–[75] : to = 0.22 μm [76] 	 <p>EP: $F \sim q$ 5 pN [72], [73] EOF: $F \sim r$ 20 pN [68]</p>	<p>$F \sim L^{-1}$</p>  <p>2 μm–1 cm [68], [75]</p>	<p>Trap?  [68]</p> <p>Steer?  [68]</p>	 [77]	 [78], [79]	Technique uses: disposable microfluidic devices, image processing, and confocal sensing.	 [68], [80], [81]

The Size of Things

Atoms range in size from 0.3 to 3 Å (1 Å = 0.1 nm = 10^{-10} m). The covalent radius of a carbon atom, half the distance between two carbon nuclei covalently bound together, is approximately 0.7 Å. Angstroms also represent the distance between H₂O molecules in water, thus it is valid to treat water (and many other fluids) as a continuum fluid in microfluidic channels. Quantum dots (QDs) are small semiconductor crystals that come in a variety of shapes and sizes. The QDs controlled in Figures 15

and 16 were ellipsoidal in shape with a 6-nm-major and 3-nm-minor axis (1 nm = 10^{-9} m). Magnetic particles for drug delivery (see [267]) range in size from 1 nm to 5 μm (1 μm = 10^{-6} m). Visible light, which sets the limit for the smallest distance that can be distinguished under a microscope, has a wavelength of 380 to 750 nm. Cells typically range in size from single micrometers (small bacteria) to 100 μm (larger mammalian cells). Human blood vessel radii range from 7 μm to 3 cm. (See Figure S1.)

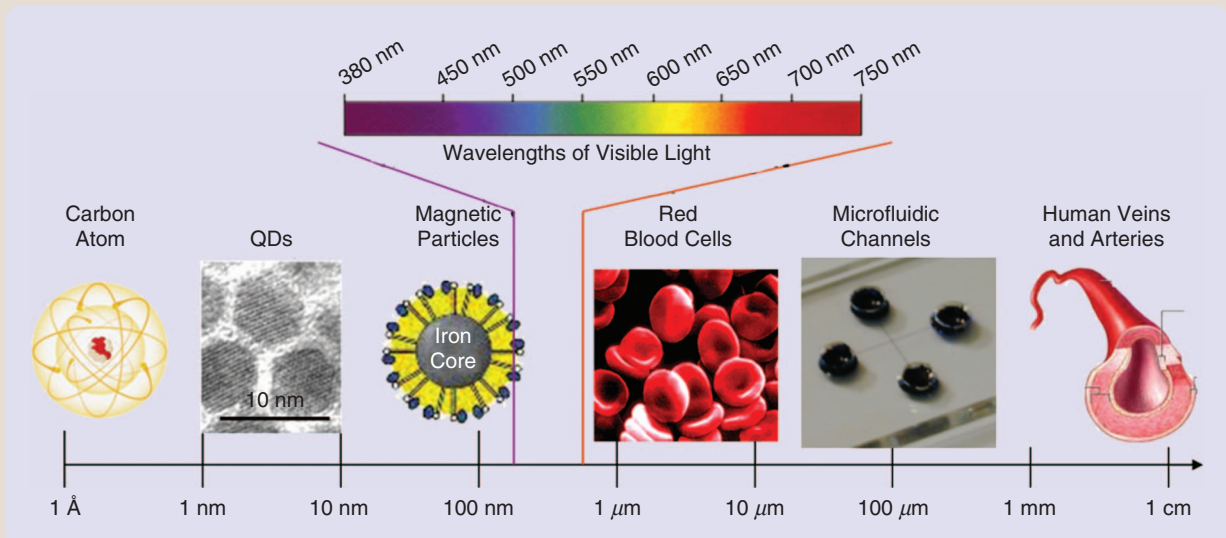


FIGURE S1 The size of objects considered in this article and in [267]. From left: carbon atom schematic, colloidal quantum dots (QDs) (tunneling electron microscope image) [266], schematic of a magnetic nanoparticle, wavelengths of visible light, red blood cells, a simple microfluidic device, and a schematic of a major human blood vessel.

Laser tweezers are sophisticated bench-top systems that require precise and expensive optical setups. Turn-key systems currently cost at least US\$18,000 (Thorlabs). A significant extension of laser tweezing is Doppler laser cooling, where ions or atoms moving forward into a laser are more likely to absorb a photon and, hence, be slowed down. Multidirectional laser Doppler cooling, in conjunction with magnetic trapping, has led to two Nobel prizes (1997 [89] and 2001 [90]) and is being extended to slowing down the motion of individual atoms [91]–[93].

Dielectrophoresis (DEP) is a common method for trapping and separating particles in microfluidic systems [38], [39], [94]–[96]. As for laser tweezers, the forces exerted on particles depend on their sizes and dielectric properties [97], [98]. Usually, many electrodes fabricated on a chip surface are actuated by high-frequency signal generators to apply spatially varying alternating-current (ac) electric fields, and serve to preferentially trap, collect, deflect, move, or rotate one type of object versus another, for example, to only capture cells of one size range [33]–[36], [40]. With the exception of more recent work [37], [42], [43], DEP has usu-

ally been applied in open loop without feedback corrections that can enable more precise control of individual objects.

Optoelectronics tweezers can generate multiple light-induced virtual DEP traps on photoconductive surfaces to manipulate thousands of polarizable particles or wires [44], [99], ranging in size from tens of nanometers to hundreds of micrometers, with submicron accuracy, in two spatial dimensions [44], [48], [49], [100]. They require chips coated with transparent conductor materials and image producing light sources [99], [101].

Acoustic tweezers were developed to overcome the inability of laser tweezers to trap optically absorbing materials [50], [53]. They use sound transducers and signal generators in combination with microfluidic devices and create stable potential wells at standing wave nodes or antinodes depending on whether the particles are more or less dense than the surrounding fluid medium [54], [102]–[104]. Acoustic tweezers have been used to trap microscale objects, such as cells, in two spatial dimensions [51]–[53], [55], [57].

Magnetic forces have also been used to control objects on chip [58]–[61], [63], [105], [106]. Unlike in [267] where we

The equations to be controlled for neutral or charged particles are linear in the control and nonlinear in the particle positions.

are interested in focusing a distributed ferrofluid of many nanoparticles to deep targets in patients, in magnetic tweezing the goal is usually to precisely manipulate single particles over short distances [58]–[61], [63], [64]. Magnetic actuation is restricted to manipulating magnetic materials, but nonmagnetic objects (such as cells) can be controlled by attaching magnetic handles [63], [64], [106], [107]. Feedback control is an integral part of magnetic tweezing and various groups have shown advanced algorithms both in theory [62], [108]–[111] and in experiments [58], [61], [62], [112]. Interestingly, magnetic and DEP actuation share the same force equations. In both cases, the force scales as the gradient of the applied field squared, $\vec{F}_{\text{DEP}} \sim \nabla(\|\vec{E}\|^2)$ and $\vec{F}_{\text{mag}} \sim \nabla(\|\vec{H}\|^2)$ where \vec{E} is the electric field and \vec{H} is the applied magnetic field. Hence, control algorithms developed for magnetic tweezing should apply equally well to precision manipulation in the DEP setting.

Electrokinetic (EK) tweezing, the subject of this article, includes both electroosmotic (EO) and electrophoretic (EP) actuations. As discussed below, electroosmosis is the actuation of fluid flow by electric fields [113], this flow can then carry along any object regardless of its dielectric or magnetic properties. Controlling flow can also be created by hydrodynamic (pressure) actuation, as in [65]–[67]. Conversely, the motion of a charged object through a medium due to an applied electric field is termed electrophoresis [114]. Unlike optical, DEP, optoelectronic, acoustic, and magnetic forces, which all scale with particle volume [30], [98], [101], [104], EP forces scale with surface charge q which usually depends on particle surface area [115] while fluid flow applies drag forces that scale with particle radius [113], [116], [117]. As particle size decreases down to the nanoscale, this scaling with radius instead of volume makes fluid-flow tweezing advantageous compared to laser, DEP, or magnetic actuation, and has enabled nanoprecise manipulation of 6 nm QDs (see the section “Manipulating Nanoscopic QDs to Nanoscale Precision”). Even high-powered laser tweezers have not been able to achieve a similar result [84].

The article is organized as follows. EO flow actuation is summarized next, along with hardware details for our microfluidic feedback control systems. The “Modeling” section first briefly reviews microfluidic modeling in general (a broad area) but then specializes to only the modeling that is necessary for EO and EP feedback control of particles. Control algorithms for manipulation of one and multiple objects are covered in the next section. This section includes theory and experimental results for steering beads and swimming cells to micrometer precision, as well as steering human

cancer cells with extended microtentacles into one another and manipulating and immobilizing QDs to nanoscale precision. A conclusion section summarizes the results, overviews emerging needs, and identifies directions for future research.

ELECTROOSMOTIC FLOW ACTUATION

Actuation of flows by modest electric fields is routine in microfluidic systems [1], [118]–[120]; a standard glass or polydimethylsiloxane (PDMS) microchannel filled with tap water and connected at its two ends to a 9-V battery exhibits EO flow (see www.controlofmicrobio.umd.edu/movies/eof-movie.mov). Electroosmosis is a fluid/solid interfacial effect that scales with device surface area and enables manipulation of flows by electric fields [113], [121]. Electrolytes such as water or cell media contain charged ions. Even ultra-pure deionized water still contains a significant amount of disassociated salts [sodium (Na^+), potassium (K^+), and chloride (Cl^-)]. When a microfluidic device is filled with an electrolyte, weak chemical reactions occur at the solid/liquid interfaces. These reactions create a net immobilized charge at the interfaces, and this unbalanced charge attracts ions of the opposite sign to create a thin layer of mobile ions in the liquid, called the Debye layer, along the surfaces of the device. The application of an electric field causes these charges to move in one direction and the thin mobile Debye layer drags the rest of the fluid along by viscous forces. Since only a few charges migrate to the surface, the interior of the channel still contains an essentially equal number of positive and negative ions (creating equal and opposite viscous forces), and no net force is created in the interior of the channel. Only the concentrated (mostly positive or mostly negative) charges in the Debye layer, on the boundaries of the channel near the surfaces of the device, create a net EO drag force, and this drag force creates fluid motion in the whole channel (Figure 2, [113], [122], [123]).

Using EO flow actuation to manipulate particles with feedback control allows simple and easy-to-fabricate devices (such as shown in Figure 3) to precisely steer and trap individual particles. If EO flow is available, then manipulation works for any visible particles, regardless of their materials or surface properties. The created forces scale favorably, with particle radius (instead of with particle volume), enabling nanoprecise control of nanoscopic objects such as QDs. In fluid/device combinations where the surface chemistry is such that EO flow does not occur or is too weak, such as for protein-rich cell-media buffers where abundant proteins coat the device walls and degrade electroosmosis, the same control algorithms have been

used to instead electrophoretically manipulate cells or particles that acquire a surface charge.

As detailed in [68], our particle control system consists of a PDMS on glass microfluidic device. Channels are imprinted into the PDMS and the PDMS layer is then adhered face down onto a glass slide. Platinum electrodes are inserted into the open-air channel-end reservoirs, through holes punched in the PDMS, to actuate the flow. The fluid filling the device can be water, cell media, or diluted blood, and the

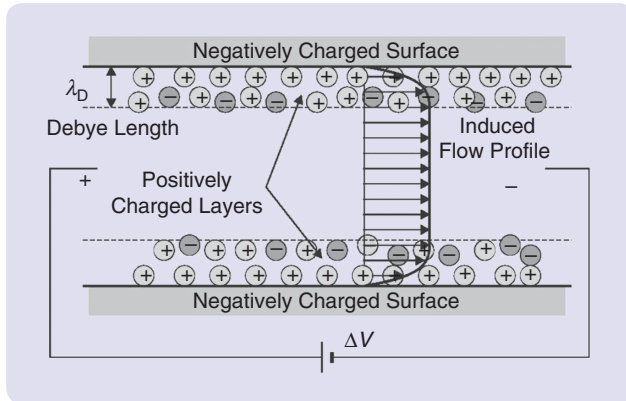


FIGURE 2 The physics of electroosmotic (EO) actuation. A schematic side view through a microfluidic channel. This channel has negatively charged surfaces, as is the case for polydimethylsiloxane channels filled with water. The \oplus or \ominus circles show naturally occurring ions in the liquid. These ions accumulate to shield the immobile charges at the channel surfaces and form a thin Debye layer that has a predominant charge (here, mostly positive). The electric field transports this Debye layer and then drags the fluid in the channel along by viscous forces. Charges in the interior of the channel (not shown) remain essentially balanced (only a small fraction of the ions shield the surfaces) and so they create no net fluid motion. The resulting fluid flow profile is shown by the black arrows, except the figure is not to scale—the Debye layer is very thin and λ_D is typically on the order of nanometers. Thus the created EO flow is essentially uniform across the width of the channel. The thin Debye layer can be treated as a moving-wall boundary condition that travels in the direction of the applied electric field [113], [120], [123]. (Figure courtesy of Anders Brask, reproduced with permission [124].)

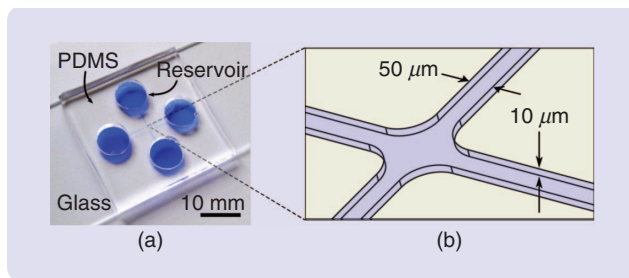


FIGURE 3 Photograph of a polydimethylsiloxane (PDMS) on glass device used for single particle control, filled with water and blue food coloring to show the microfluidic channels and reservoirs. Each microchannel is 10- μm deep, 10-mm long, 50- μm wide close to the particle steering intersection region, and 300- μm wide otherwise. The zoom shows a schematic of the channel intersection and the 100 μm \times 100 μm particle steering control region.

objects to be controlled can be any small optically visible particles, such as beads, cells, wires, or light-emitting QDs. The real-time location of the objects is sensed by a vision system that consists of a microscope, camera, and in-house imaging software. It includes a $\times 40$ magnification transmitted-light microscope (Nikon TS100), a 40 frame/s 480 by 640 gray-scale pixel camera (Vision Components, VC2038E DSP, Ettlingen, Germany), and a digital signal processing (DSP) unit located inside the camera that evaluates the particle-tracking algorithm. The control algorithms are implemented on a personal computer (a Dell Precision Workstation 530, Xeon 1.7 GHz, 2 GB memory, WinXP) and the resulting actuation commands are sent to a multichannel digital-to-analog signal converter (National Instruments DAQ) to actuate up to 16 electrodes with ≤ 10 V each. The range of actuation voltages used depends on the desired particle control speed, device channel lengths, buffer used, and particles to be steered (for example, lower voltages are preferred to manipulate fragile live human cells [125]–[128]), but the voltage range is always modest, up to 50 V for control of QDs, ≤ 10 V for manipulation of cells, and ~ 1 V for devices that have been optimized to create stronger flows at low voltages [69], [129].

MODELING

Modeling of microfluidics is a broad area and is discussed in multiple books [118], [122], [123], [130]–[133]. Generally, bulk flows in microfluidic devices can be considered as continuum liquids. For example, water at room temperature consists of closely packed H_2O molecules separated by angstrom distances [134]. This separation distance sets the mean-free path of the molecules λ and, when compared to micrometer channel dimensions, yields a Knudsen number $Kn \approx \lambda/L < 10^{-4}$ which is well within the continuum regime [1], [130]. Noncontinuum fluid effects do occur when the dimensions of the channels begin to approach the size or separation of the particles making up the liquid, for example for nanowidth channels [135], but in most situations a continuum description of the bulk flow suffices.

As the device length scale L decreases, volume $V \sim L^3$ shrinks faster than surface area $A \sim L^2$ and, hence, surface effects generally dominate bulk phenomena on the microscale [122], [130], [135]. Specifically, fluid momentum is proportional to volume and is almost always negligible compared to surface effects in microfluidic systems [1], [119]. Thus, for incompressible liquids like water, the incompressible Navier Stokes equations ($\nabla \cdot \vec{V} = 0$, $\rho[\partial \vec{V}/\partial t + \vec{V} \cdot \nabla \vec{V}] = -\nabla P + \mu \nabla^2 \vec{V}$) can be reduced to the Stokes equations ($\nabla \cdot \vec{V} = 0$, $\rho \partial \vec{V}/\partial t = -\nabla P + \mu \nabla^2 \vec{V}$) [136]. The time derivative term $\rho \partial \vec{V}/\partial t$ can also usually be neglected unless the external actuation is very fast compared to local fluid momentum [137], [138], further simplifying the description of the bulk flow to the incompressible Hele-Shaw equations ($\nabla \cdot \vec{V} = 0$, $\mu \nabla^2 \vec{V} = \nabla P$) [139]. Unlike the Navier Stokes equations, both the Stokes and the

EOF control manipulates particles by fluid drag forces that scale with object radius (instead of volume) and thus enables nanoprecise manipulation of nanoscale objects.

Hele-Shaw equations are linear, which substantially simplifies their solution.

Surface effects, such as electroosmosis and surface tension, act as boundary conditions for bulk flows on the microscale [123], [140]. They can be exploited to actuate micro flows, for instance by electroosmosis [123], [141]–[143], surface tension [144] (which can be electrically [145] or thermally modified [146]), by evaporation [147], or by other surface phenomena [1], [140]. Behavior at surfaces can be subtle, surprising, and difficult to understand and quantify. Electrowetting, where applied voltages change the shape and location of liquids [145], [148]–[155], is a good example. Electrowetting has been used to move, join, split, merge, and mix liquids on chip [45], [152], [154], [156]–[160], as well as to change the shape of liquid lenses for cell phone camera focusing [161], [162] and to enable thin and flexible video-speed color displays [163]–[166]. Substantial effort was required just to understand which physical phenomena create the effect. It is now recognized that electrowetting is driven primarily by a competition between electric energy storage in the underlying solid dielectric versus surface tension energy at the solid/liquid and liquid/gas interfaces [145], [167]. There is an active electrowetting research community, with many articles on modeling both the basics and the details of electrowetting [138], [153], [165], [166], [168]–[183]. Other surface effects have their own underlying physical phenomena and mathematical descriptions: for example, see [120] and [123] for modeling of electroosmosis and electrophoresis; see [113] and [121] for an introduction to quantifying surface tension with [184] and [185] for further modeling thermally induced surface tension motion (the Marangoni effect); and see [186] for modeling of flow velocities created by liquid evaporation. Many of these models can be computationally expensive, so care must be taken either to build models that are tractable for control design (as done in [187] for electrowetting) or to reduce the computational complexity by model reduction techniques [188]–[191], as done in [192]–[194] for microflows.

In addition to the importance of surface phenomena, microfluidic devices often contain objects (such as particles, wires, DNA, and living cells) that have their own additional dynamics within the flow and can be preferentially actuated by applied electrical, optical, magnetic, or other means. All such small objects undergo Brownian fluctuations [195], with smaller particles experiencing greater motion (by the Einstein-Stokes relation for spherical particles at low Reynolds numbers, the diffusion coefficient is $D = kT/6\pi\mu a$ where a is the radius of the particle, k is the Boltzmann constant, T is the

absolute temperature, and μ is the fluid viscosity [116], [117]). Self-consistent simulation of stochastic dynamics is discussed in Gillespie [196] and Brownian motion can be added as random walks to particle convection models (as in [197]). For nonspherical rigid objects, such as wires, rotational diffusion must also be included [76], [198], [199] and interaction with channel surfaces can become an issue [200]. DNA strands, which act as elastic threads, are heavily studied and there is rich literature on the dynamics of DNA in free and confined spaces [132], [201]–[204]. Live swimming cell motion depends on the type of organism. For example, the probability of different *E. coli* motion patterns has been quantified, modeled, and compared to experiments in [205] and [206]. Finally, depending on their electrical, optical, and magnetic properties, objects in the liquid can be actuated by externally applied fields. Such actuation capabilities were summarized in Table 1 and modeling of these actuation methods can be found in [83] and [84] for laser tweezers; in [42], [43], [97], and [98] for DEP; in [101] and [207] for optoelectronics; and in [51], [54], and [102]–[104] for acoustic and magnetic [62], [108], [109], [111], [208] actuation.

Modeling Electroosmotic Actuation and the Resulting Particle Motions

For modeling the EO manipulation of particles, there are three key phenomena that need to be included: low Reynolds number fluid flow, electric fields (including how they actuate flow), and particle Brownian motion. There is also pressure flow caused by surface tension imbalances between the reservoirs, but this flow acts as a disturbance (see the section “Experimental Results for Multiparticle Control to Micrometer Precision”), it does not couple to EO flow (the two can be solved independently by the linearity of Stokes or Hele Shaw flow) [113], [122], and pressure flow does not affect the design of the least-squares control algorithms. The goal of the modeling is to find the mapping from electrode actuations to the resulting particle motions.

In two-dimensional devices, such as the one shown in Figure 3, the created EO flow is planar. As illustrated in Figure 2, mobile charges that accumulate at the device surfaces (at the floor, walls, and ceiling of the microfluidic channels and chamber) are transported by the applied electric field and drag the fluid along by viscous forces. Thus, at each surface location, EO flow is actuated in the direction of the applied electric field. This electric field is created between electrodes inserted into the four fluid reservoirs and remains inside the conducting fluid (the PDMS device

material is insulating). The electric field is uniform in the vertical direction but can vary in the horizontal plane and in time. It can be shown rigorously by analyzing the Navier Stokes equations [197] that the EO flow aligns quickly, in microseconds [197], [209], with the electric field. Hence,

$$\vec{V}(x, y, z, t) = (\varepsilon\zeta/\mu) \vec{E}(x, y, t) = -(\varepsilon\zeta/\mu) \nabla\phi(x, y, t) \quad (1)$$

where \vec{V} is the EO fluid velocity, \vec{E} is the applied electric field, ϕ is the electric potential (as created by the four electrodes), ε is the permittivity of the liquid, μ is its viscosity, and ζ represents the zeta potential (voltage) at the liquid/device interfaces [113], [121]. It is ζ that quantifies the amount of charge contained in the Debye layer [113], [121], [122]. Since this zeta potential depends on the detailed chemistry of the fluid and the device surfaces, it is not predicted a priori but is instead inferred from experiments by applying a known electric field and measuring the resulting flow velocity [210]. An example planar EO flow field governed by (1) is illustrated schematically in Figure 1.

Neutral particles inside the fluid are convected by the created EO flow and also undergo Brownian motion. When the particles are comparable in size to the channel height (for example, the yeast cells that are $\sim 5 \mu\text{m}$ in diameter compared to the $11\text{-}\mu\text{m}$ -high channels in [68]), they often come in contact with the floor and ceiling of the device. When the particles are smaller, the 6 nm QDs, for example, then they can diffuse unobstructed in all three directions [unless other factors, such as chemical separation, cause them to remain at a surface (see the section “Manipulating Nanoscopic QDs to Nanoscale Precision”). Below, only the horizontal xy motion is controlled allowing the particles to move freely in the z direction. Their in-plane positions are governed by convection plus diffusion, by

$$\dot{\vec{P}}_j = \vec{V}(\vec{P}_j) + \vec{w}$$

where \vec{P} is the vector of particle x and y locations, \vec{w} is Brownian noise, and $\vec{V}(\vec{P}_j)$ is the EO fluid velocity at the j th particle location.

The electric field obeys Laplace’s equation $\nabla^2\phi = 0$ [211] with Dirichlet boundary conditions at the electrode boundaries $\phi(\partial D_j) = u_j$ where ∂D_j denotes the liquid/electrode surface and u_j is the j th applied voltage. The PDMS material is insulating, hence Neumann boundary conditions hold at the liquid/device surfaces. The solution of Laplace’s equation is linear in the applied voltages, hence,

$$\begin{aligned} \dot{\vec{P}} &= \vec{V}(\vec{P}) + \vec{w} = c\vec{E}(\vec{P}) + \vec{w} = -c \nabla\phi(\vec{P}) + \vec{w} \\ &= -c \sum_{j=1}^n \nabla\phi_j(\vec{P}) u_j + \vec{w} \end{aligned} \quad (2)$$

where $c = \varepsilon\zeta/\mu$ is the EO mobility of the fluid, ϕ_j is the solution to Laplace’s equation when electrode j has a unit applied voltage and all the other electrodes are set to zero, and $\vec{u} = (u_1, u_2, \dots, u_n)$ is the time-varying vector of applied voltages.

The same type of surface chemistry that causes Debye layers to form at device surfaces also allows particle surfaces to become charged [113], [121], [212]. An added electrostatic force acts on such charged particles and creates an additional steady-state EP velocity. This EP velocity points either exactly along or exactly against the local electric field, depending on the sign of the surface charge. Thus the effect of particle surface charge can be incorporated into (2) by modifying the mobility coefficient c to be the sum of the EO and EP mobilities for each particle [113]. If different particles have different surface charges, as can occur in experiments, then each particle has its own mobility coefficient c_i and this introduces m mobility coefficients into (2).

Putting all of the above together, the equations to be controlled for neutral or charged particles are linear in the control and nonlinear in the particle positions. They are

$$\dot{\vec{P}} = A(\vec{P}) \vec{u} + \vec{w} \quad (3)$$

where $\vec{P} = (x_1, y_1, x_2, y_2, \dots, x_m, y_m)$ is the position vector for the horizontal locations of the m particles of interest and the $m \times n$ sized A matrix contains spatial information about the electric fields originating from each of the n electrodes.

The above model is simple. It neglects effects that do occur in the devices such as parasitic pressure flows (caused by meniscus surface tension imbalances between the n electrode reservoirs), possible contact of particles with the device surfaces, and the details of the Debye charge layer formation. The model also contains a significant amount of uncertainty, such as buffer chemistry and cell-to-cell variations that can cause the zeta potential and particle surface charges to vary by $\pm 50\%$, as well as uncertainty due to channel fabrication imperfections and PDMS surface waviness [68]. Yet this model is effective. It has proven sufficient to enable fast and gentle control of live cells in complex biological media [68], [69] and to position nanoscopic particles on chip with nanoscale precision [71], [72]. The model is good enough to enable effective feedback correction—it correctly predicts electric field and flow *directions* and therefore enables a choice of electrode actuations that directs the particles closer to where they should be at each control update. During closed loop control, manipulation errors are dominated by particle diffusion between control updates and vision sensing noise, and these two factors can be reduced to tens of nanometers [72].

CONTROL

The goal of the control is to manipulate, steer, and hold individual particles in the microfluidic devices. In this section, algorithms are developed and results are demonstrated in experiments for the control of one and multiple objects on chip to micrometer and nanoscale precision.

Single Particle Control

Control design for a single neutral or charged particle in a four-channel device is straightforward. Flow is always

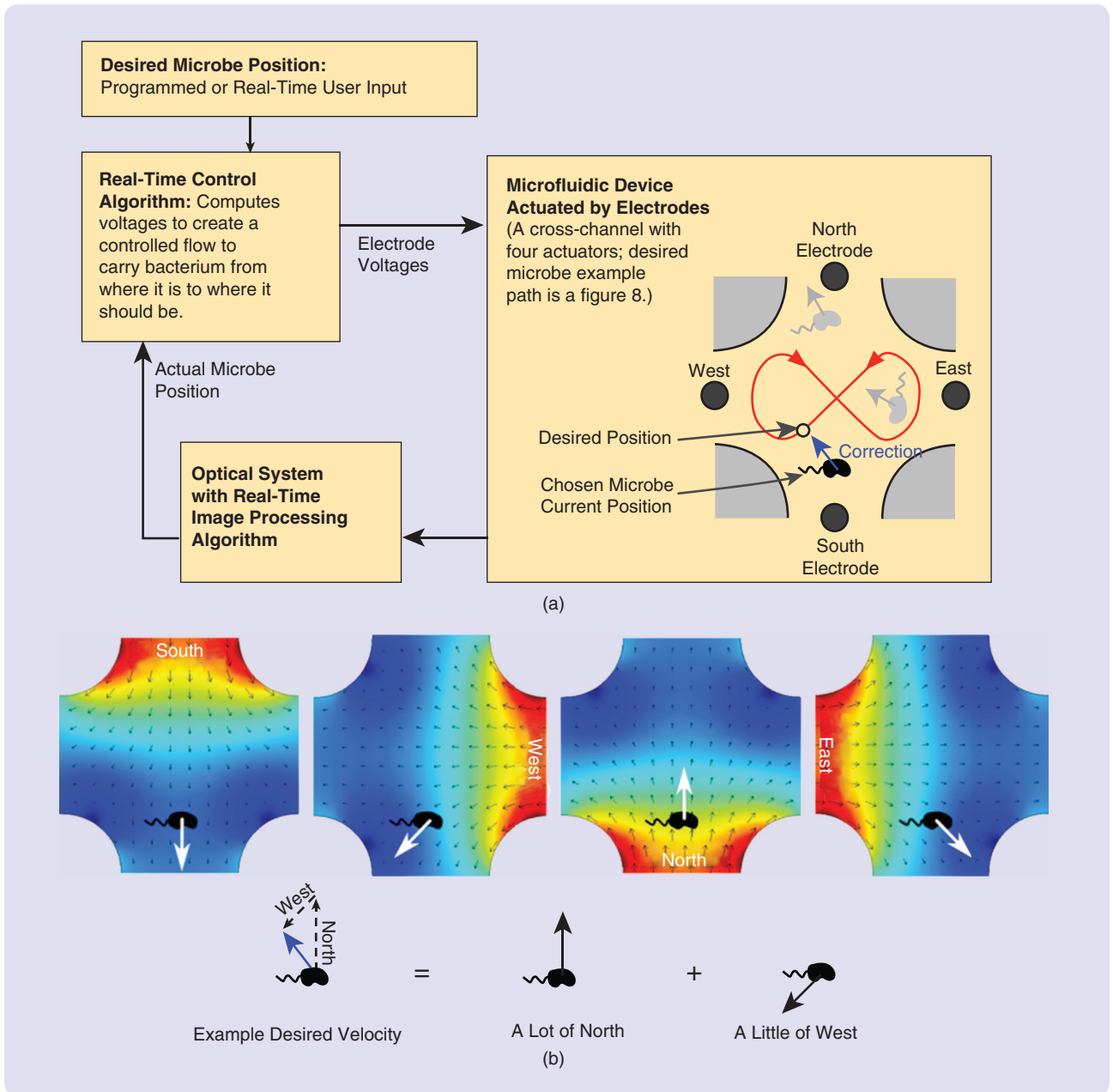


FIGURE 4 The feedback loop and control scheme for steering a single object, here a swimming bacterium [68]. (a) To steer a single microbe along an ∞ path, the control region of the four-channel microfluidic device is observed by an optical system that monitors the location of the chosen bacterium in real time. The controller compares the measured location (black bacterium) against its desired position (open circle) and commands a flow to move that bacterium from one location to the other. The other bacteria are also actuated (gray arrows), but only the chosen microbe is steered back to its target location. (b) Simulated fluid flows are shown for each of the four electrode actuations (arrows show the flow field, color shows the electric potential). The flows spread out as shown, each creating the velocity shown by the white arrow at the bacterium's current location. Correctly scaling and adding these four flows together can create any desired velocity at any bacterium location.

created from the observed to the desired particle location. If the particle is to the southeast of its desired position, a correcting northwest flow is applied. The feedback control loop is shown in Figure 4. The microfluidic device of Figure 3 is observed through a microscope and a camera. Real-time image detection software tracks the location of one chosen object, in this case a live swimming microbe,

through a field of many others. The control then creates a flow to move that microbe as needed. (The flow at the particle's location is a linear superposition of the four flows created by each electrode alone, due to the linearity of Laplace's equation. As shown in the figure, these four flows can be combined to create a correcting flow at the particle's location in any desired direction.) The vision sensing and

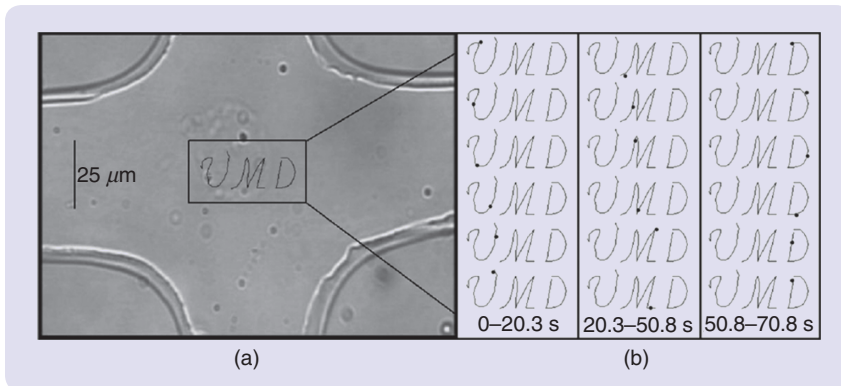


FIGURE 5 Steering of a yeast cell with modest surface charge along a “UMD” path (for the University of Maryland) [68]. (a) Photograph of the device control region, with the UMD path overlaid on the image, showing visible imperfections in the device surface and walls. (b) The path of the chosen 5- μm yeast cell (black dot) in the experiment. Snapshots are shown at six equally spaced times for each letter. (The electroosmotic mobility of the fluid is $c_{eo} = (36.5 \pm 3.6) \times 10^{-9} \text{ m}^2 \text{ V}^{-1} \text{ s}^{-1}$, the electrophoretic mobility of the charged yeast cell is $c_{ep} = (-23.3 \pm 6.9) \times 10^{-9} \text{ m}^2 \text{ V}^{-1} \text{ s}^{-1}$). This cell does not swim and is steered with a 1 μm accuracy. (Movie available online at www.controlofmicrobio.umd.edu/movies/cell-on-UMD.mov.)

velocity correction repeats again at the next time to continuously correct errors caused by particle diffusion and, in this example, also by bacterium swimming.

Although the control algorithm described above is straightforward, experimental results for manipulation of a single particle required the solution of practical issues. These included optimal device fabrication, fast and reliable vision sensing, prevention of device fouling (cells can stick to device surfaces), and operation of the device in a regime with strong and reliable EO actuation but an acceptable level

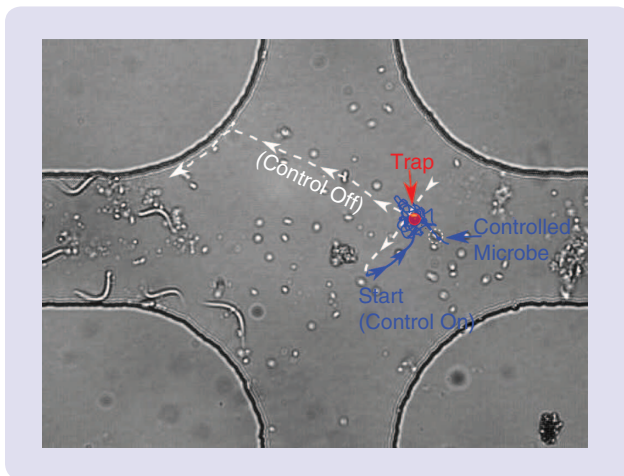


FIGURE 6 Flow control of a swimming microbe found in river water. The microbe was moved to and trapped at the red dot location for 30 s until being released from control. Initial uncontrolled swimming is shown in dashed white, subsequent controlled motion is shown in blue. The microbe swims away after control is turned off (dashed white again) indicating it was not harmed by the flow control. (Movie available at www.controlofmicrobio.umd.edu/movies/swimming-cell.mov.)

of electrolysis (a chemical reaction that occurs at the electrodes and creates visible bubbles [213], [214] which, if produced in excess, can disrupt the flow control). The engineering solution of these issues can be found in [81], which reports the first successful experiments on trapping and steering single non-swimming cells by feedback flow control (Figure 5).

For control of swimming species, so long as the feedback can correct the location of the microbe faster than that microbe can swim away, it will succeed in trapping and steering the microbe. The difficulty level of doing this depends on both the swim speed of the microbe and its swim patterns. Fast swimming microbes that tend to swim in small circles can be controlled more easily because, even though they swim quickly, they do not swim far

away. In contrast, medium-speed microbes swimming in straight lines in random directions travel further away and are more difficult to retrieve. Figure 6 shows initial results for manipulation of medium-speed ($< 10 \mu\text{m/s}$) swimmers. The control in this case is updated slowly, every 1/30th of a second. The next generation system will implement flow control at 300 Hz and will further optimize device design to increase EO flow speeds so as to effectively steer and trap even fast swimmers.

Control Algorithm for Multiparticle Manipulation

In addition to control of a single object, it is possible to manipulate multiple particles independently using flow control [68]. A device with n electrodes can actuate $n - 1$ flow modes (one electrode corresponds to ground). Different modes cause particles in different locations to move in different directions (Figure 7). The modes are found by decomposing the A matrix of (3), where for the purpose of computing the modes the vector \vec{P} is replaced by a fine mesh of points, into its singular value decomposition (SVD). The first SVD mode of A corresponds to the strongest fluid flow mode that can be created with minimal electrical actuation, the second SVD mode corresponds to the second strongest fluid mode, and so on. By judiciously combining such modes during control, it is possible to simultaneously move multiple particles in multiple desired directions.

The multiparticle control algorithm works by least squares [197]. Define the desired correction velocity vector to point from the observed locations of the chosen particles toward their desired locations as follows:

$$\vec{v}_{\text{correction}} = k(\vec{P}_{\text{desired}} - \vec{P}_{\text{observed}}). \quad (4)$$

Here, k is a scalar control gain. The goal is to choose the voltages at the electrodes to create a velocity as close to this desired correction velocity as possible. By (3), for the current measured particle positions, a linear relation exists between the applied voltages and the particle velocities. Since this velocity is achieved as soon as the voltages are applied, it suffices to solve a static linear problem to determine the needed set of electrode voltages. This is done by least squares and gives the control algorithm

$$\begin{aligned} \vec{u}^* &= [A^T(\vec{P}) A(\vec{P})]^{-1} A^T(\vec{P}) \vec{v}_{\text{correction}} \\ &= k[A^T(\vec{P}) A(\vec{P})]^{-1} A^T(\vec{P}) (\vec{P}_{\text{desired}} - \vec{P}_{\text{observed}}). \end{aligned} \quad (5)$$

For the case where there are more actuations than particle degrees of freedom ($n - 1 \geq 2m$), the A matrix typically has full row rank (unless two particles are at the same location) and the above least squares answer achieves the desired velocity with minimum control effort $\|\vec{u}\|_2$. For cases where there are more particles than actuation degrees of freedom, the experimental performance rapidly degrades to unusable. For example, four particles (eight degrees of freedom) can be controlled only somewhat by eight electrodes (seven degrees of freedom, one electrode is ground), but five particles cannot. Since it is possible to fabricate devices with many electrodes, the number of usable fluid modes (explained next) determines the practical limit to the number of particles that can be controlled.

The electric fields that make up the A matrix are computed ahead of time, providing a reference table to compile A for any particle positions \vec{P} captured by the camera. The pseudoinverse $(A^T A)^{-1} A^T$ is then computed in real time (milliseconds) as the control proceeds. It is advantageous to carry out this calculation in the coordinate system of the fluid modes of Figure 7 (the singular value modes of the matrix A evaluated on a fine grid of points). The lower spatial frequency modes are better conditioned; higher spatial modes require high voltages to create even small fluid velocities. The matrix A is truncated onto the lower SVD modes and the pseudoinverse is computed for this well-conditioned matrix. Actuation is kept below the maximum allowable voltages in one of two ways: either by turning down the control gain per particle as the voltage limit is approached or, more rigorously, by phrasing a linear-programming constrained optimization to choose the gain per particle to maximize performance but not exceed actuator limits. These two approaches work equally well in experiments. In current devices, which have been optimized over the last five years, it is possible to reliably access the first ten fluid modes, thus allowing simultaneous control of up to five particles. Higher spatial frequency modes are too weak to overcome the parasitic pressure flow disturbances that still remain in these devices.

The least squares control algorithm above can also be used to manipulate particles in three dimensions (3D)

and to control object orientations. Multilayer devices that create flow modes with a vertical component from one layer to the other enable 3D manipulation [215]. Modulation of flow shear, in addition to flow translation, enables control of object rotation [76]. In both cases, the dynamics is still described by the structure of (3) but the \vec{P} vector now further includes either the vertical position of the particles or the orientation of the objects. Either way, the control law of (5) remains valid. So far, 3D and rotation control capabilities have been verified in simulations and some preliminary experiments but have not yet been published.

Experimental Results for Multiparticle Control to Micrometer Precision

The control law of (5) has been implemented on devices with more than four electrodes (usually eight, sometimes 12 or 16) to manipulate multiple particles at once [68]. Figures 8 and 9 show results for steering three particles using eight electrodes, still to 1- μm accuracy as in Figure 5 for a single particle. The control of four and five particles at once has also been demonstrated, but the manipulation accuracy was degraded to 5 μm [129].

An interesting issue, relevant for testing cell-to-cell interactions, is how close flow control can bring two particles together. Doing so is challenging because it requires

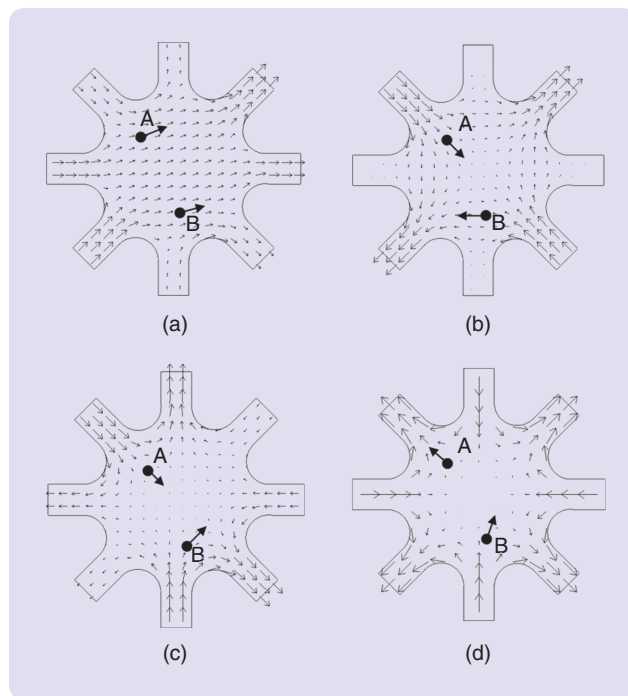


FIGURE 7 Electroosmotic microflow modes for an eight-electrode device. The above figure shows the first, third, fifth, and seventh modes computed from the model stated above (also see [68] and [197]). The two example neutral particles A and B (shown as black dots above) then experience the velocities shown by the arrows [68]. (a) Fluid mode one, (b) fluid mode three, (c) fluid mode five, and (d) fluid mode seven.

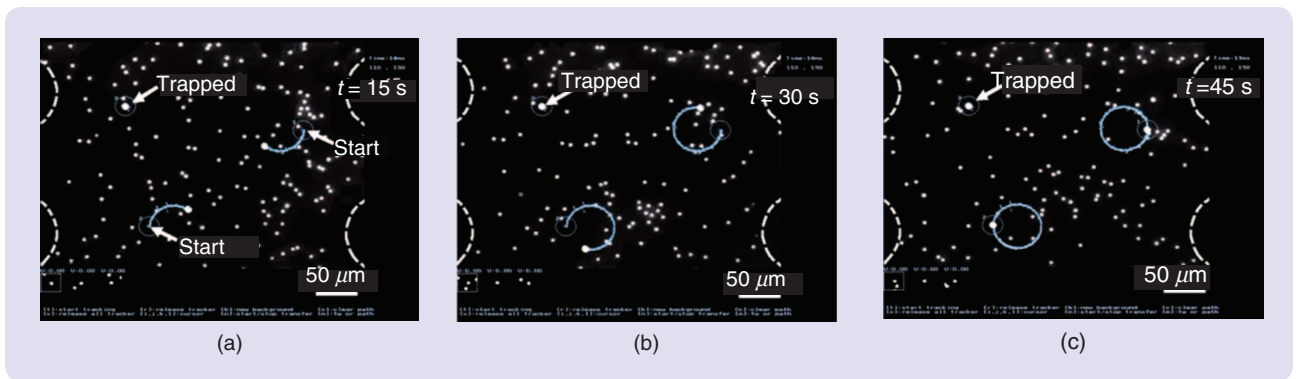


FIGURE 8 Flow control of two fluorescent beads (2.2- μm diameter) around two circles while a third bead is held stationary. Here the white dots are the beads (enlarged), the blue curves are the actual trajectories that the chosen beads have traced out (overlaid), and the dashed white curves (also overlaid) show the geometry of the channels and the particle control chamber. Snapshots are shown at three time steps. The two beads are being steered to within an accuracy of one pixel (corresponding to less than 1 μm). The desired paths are not shown because, at this image resolution, they would perfectly underlay the actual paths. The trapped bead is marked by an arrow and has been trapped by the control algorithm to an accuracy of better than one micron. Every time the bead deviates from its desired position through Brownian motion, the electrodes create a flow that pushes the bead back toward its desired location [68]. (Movie available online at www.controlofmicrobio.umd.edu/movies/1trap-2circle.mov.)

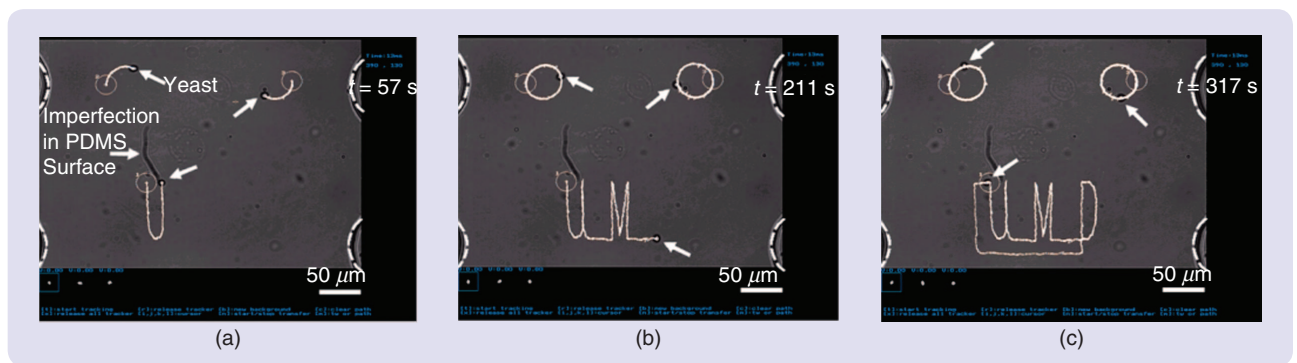


FIGURE 9 Flow control of three yeast cells (5 μm diameter) with modest surface charge around two circles and a UMD path. The yeast cells are visible as small black dots with a white center (the three target cells are marked with a white arrow in each image) and the white curves are the trajectories that the target cells have traced out. The three cells are being steered to within an accuracy of one pixel (corresponding to less than 1 μm) [68]. (Movie available online at www.controlofmicrobio.umd.edu/movies/1UMD-2circle.mov.)

creating opposing flows at two nearby points a and b to bring the two particles closer toward each other ($a \rightarrow \leftarrow b$). The A matrix of (3) has two rows per particle, and each pair of rows gives the mapping from electrode voltages to the x and y fluid velocity at that particle's location. When two particles are nearby, they experience similar fluid flows, the two pairs of rows are almost linearly dependent, the A matrix becomes ill-conditioned, and the pseudoinverse in the control law of (5) commands high voltages. For the results in Figure 10, actuation voltages were limited to 10 V by amplifier hardware, and this allowed bringing two 5 μm diameter particles to within 8 μm of one another (as measured center to center). Particle-to-particle steering is currently being improved by a control algorithm modification; instead of controlling the absolute position of two particles along two paths (four controlled degrees of freedom, as in Figure 10), the modified control algorithm acts only to reduce the linear distance between two particles (a single degree of freedom)

at each time. Higher voltages, which enable stronger opposing flows for two nearby particles, are being enabled by using a more powerful amplifier as well as by incorporating gel electrodes that delay the onset of electrolysis [216]–[218].

Finally, Figure 11 illustrates the global stability of the control algorithm of (5) and its ability to bring particles back to their targets even after large deviations. The particle control algorithm works robustly across the entire control region. There are no combinations of particle locations where it is not possible to reliably pseudo-invert A (except, as noted above, when steering two particles to the same position or attempting to steer two particles at the same location in two different directions).

In summary, PDMS devices with 4–16 electrodes, a vision system consisting of a camera, microscope, and in-house software, and least-squares feedback control algorithms have trapped and steered particles and cells to single micron accuracy. The vision algorithm can track

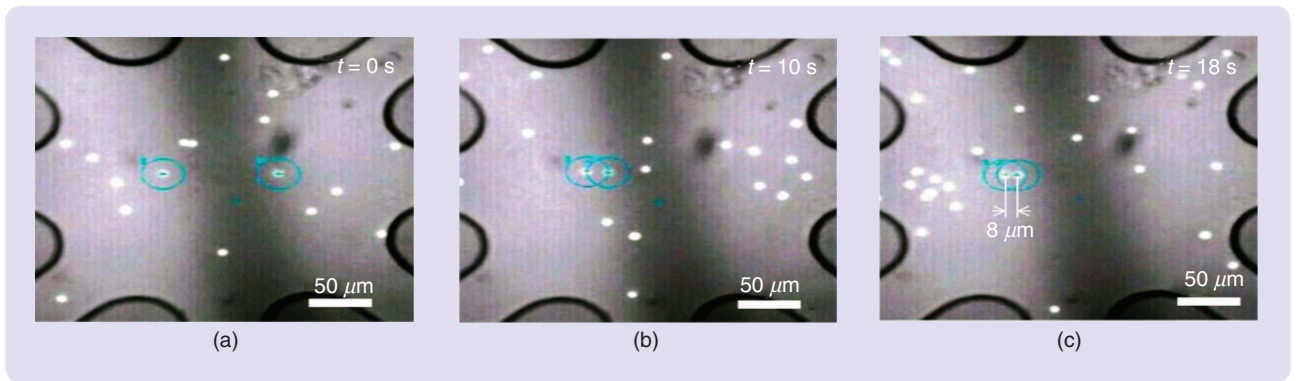


FIGURE 10 Bringing two 5- μm beads together by flow control. With the 10-V actuator limits of this experiment, the beads could repeatedly be steered to within 8 μm of one another. (Movie available online at www.controlofmicrobio.umd.edu/movies/particle-to-particle.mov.)

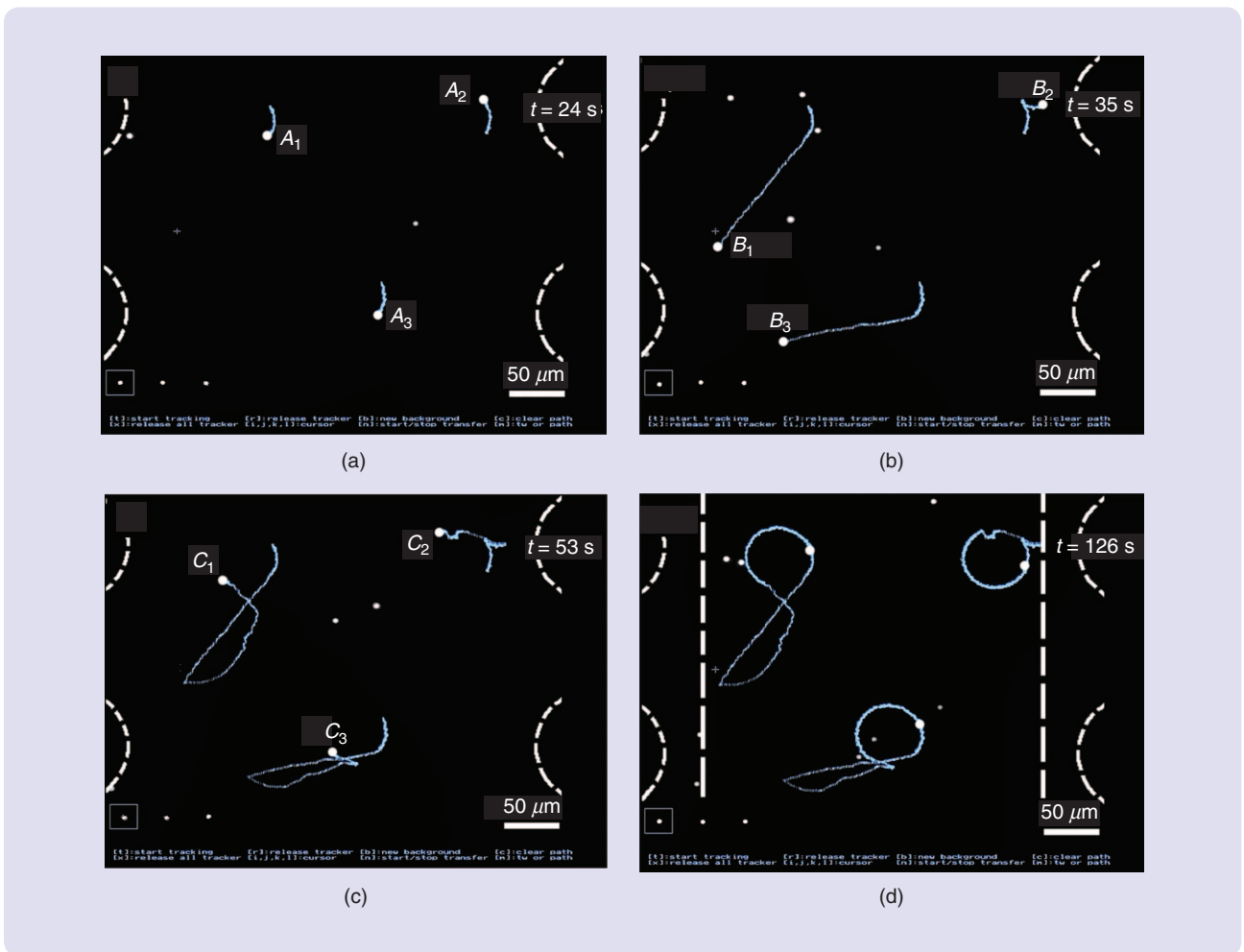


FIGURE 11 The least-squares flow control algorithm is globally stable and can correct large errors in particle positions. This figure shows steering of three fluorescent beads (2.2 μm diameter) around three circles. At time $t = 24$ s, corresponding to bead positions marked A_1 , A_2 , and A_3 , the control was turned off for 11 s, allowing the particles to drift away by up to 150 μm . (Drift is due to the parasitic pressure flow inside the device caused by misbalanced surface tension forces at the reservoirs.) The control was reactivated at $t = 35$ s (bead positions B_1 , B_2 , and B_3), and the control algorithm steered the three original beads back to their desired positions (C_1 , C_2 , and C_3). Four time instants are shown: (a) right before control is turned off, (b) right before control is turned back on (the three beads have drifted away a significant distance), (c) when the beads are back on track, and (d) when the beads have completed the remainder of their three circular paths (once again to an accuracy of better than 1 μm). The two dashed straight lines in the last image illustrate the left and right boundaries of the control region [68]. (Movie available online at www.controlofmicrobio.umd.edu/movies/global-stability.mov.)

individual particles through a field of thousands of others and with current device fabrication and voltage actuation limits can control up to five chosen particles simultaneously. Flow control can manipulate any visible particles regardless of their material properties while EP actuation requires surface charge but still works if different particles acquire different amounts of charge. For the experiments presented above, the particles were free floating with

uncontrolled vertical motion, but particles can also be restricted to the chip surface by fluid chemistry (as in the section on manipulating QDs) or their motion can be controlled in all three dimensions by using multilayer devices that can create fluid flows or electric fields with vertical components [215]. Controlled particles can range in size from micrometers to nanometers—as discussed in the next two application sections on manipulating $\sim 20 \mu\text{m}$ live

human tumor cells and 6 nm diameter QDs. The manipulation accuracy is set by the vision-sensing error plus the amount particles diffuse between control updates. This manipulation accuracy is optimized for nanoscopic particles below and is driven down to nanometers by subpixel imaging and a high-viscosity fluid that reduces Brownian motion. The current system can move particles at velocities of up to $\sim 500 \mu\text{m/s}$ with a control update rate of 40 Hz, a rate that is being increased to 300 Hz to enable control of fast-swimming microbes and to quickly assemble nanoscopic components on chip. The next two sections describe how this system is being extended to address two key applications: 1) manipulation of live human cancer cells to study their behavior in response to drugs and each other, and 2) nanoprecise control of QDs on chip to fabricate multidot nanophotonic systems.

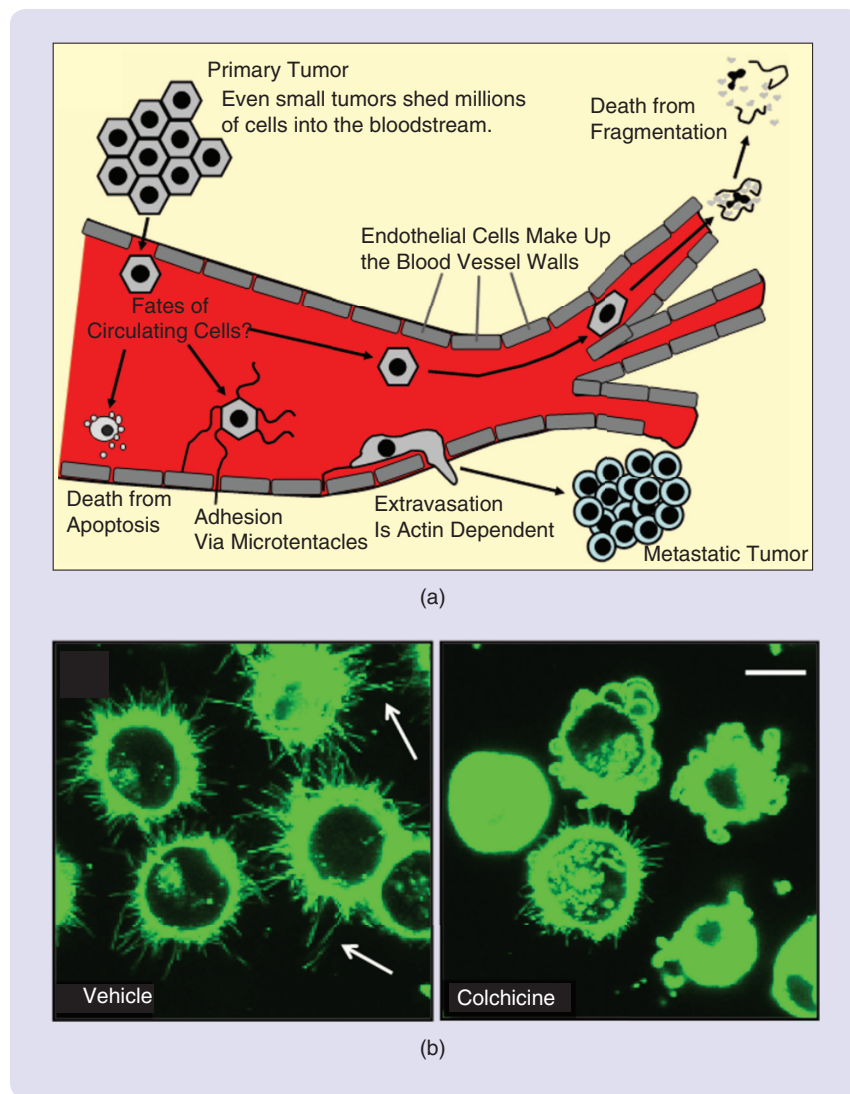


FIGURE 12 Seeding of metastatic tumors by shed circulating tumor cells (CTCs). (a) The possible fates of CTCs. Many CTCs that are shed from primary tumors either die by programmed cell death (apoptosis) or fragment when they are pushed through narrow capillaries by blood flow. But some CTCs reattach to blood vessel wall endothelial cells using microtentacles (McTNs) and escape blood vessels through actin-dependent crawling. Both steps are thought to be required to successfully form a metastatic tumor. (b) As an in-vitro model of CTCs, free-floating human MDA-436 cultured breast-tumor cells extend McTNs (left panel, white arrows) that are visible when cells are labeled with green fluorescent protein and treated only with a drug vehicle [0.1% Dimethyl sulfoxide (DMSO), here used as a chemical penetrant to transport materials into cells]. In contrast, treatment with DMSO and a tubulin-disrupting drug (Colchicine, $100 \mu\text{M}$, 10 min) causes the shortening and collapse of McTNs (right panel, scale bar $10 \mu\text{m}$). (Figure courtesy of Stuart S. Martin, University of Maryland School of Medicine.)

An emerging application for on-chip EO/EP control is monitoring and testing live human circulating tumor cells.

existing chemotherapies that target cell division [223]. In addition, even the most advanced clinical imaging methods can only detect tumors in patients when they form foci of more than 5 million tumor cells [224]. As a consequence, current cancer diagnosis and drug development is aimed at large tumors rather than the disseminating tumor cells that cause metastatic spread. As many as 30–50% of cancer patients who show no evidence of clinically detectable metastasis have CTCs that can be isolated from their bloodstream, and these strongly predict an increased risk of metastatic progression and death from cancer [225], [226]. The ability of CTCs to resist traditional therapies and remain undetectable to clinical imaging makes them one of the most elusive targets in cancer treatment. So while the great majority of current cancer research and drug development has focused on inhibiting tumor growth or reducing the invasion and motility of already attached tumor cells [227], [228], comparatively little is known about therapeutic targets for circulating tumor cells or the effects of existing chemotherapies on CTCs.

Recent studies have revealed that detached and circulating tumor cells produce microtentacles (McTNs) that penetrate blood vessel wall endothelial layers and promote tumor cell reattachment [229]. Genetic alterations that increase McTNs are known to enhance the retention of CTCs in distant tissues during metastatic spread [230], [231]. McTNs are long extensions of the cell membrane that arise when the forces of outward microtubule extension from the cell center overcome the inward tension of the actin cortex that lies beneath the cell plasma membrane [232]. When tumor cells attach to the extracellular matrix or to man-made surfaces (such as glass slides or lab-on-a-chip surfaces), increasing tension in the actin cortex suppresses microtubule extension [233], [234] and, hence, McTN formation [229], [235]. For this reason, McTNs are only detectable on detached and free-floating tumor cells [229], [235], which has led to McTNs being overlooked in many previous studies and has complicated the use of microscopy to image them.

Common cancer treatments stabilize tubulin to prevent tumor cell division (taxanes) or disrupt actin to reduce local tumor invasion (Rho and Src inhibitors). However, such cytoskeletal disruptions can elevate levels of CTCs in the bloodstream by more than 1000-fold [236], [237]; increase the number and length of McTNs [229], [238]; and promote the attachment and retention of CTCs at distant sites in the body [230], [231]. Developing methods to

manipulate and analyze free-floating tumor cells is essential so that microscopy can be used to better understand the effects of drug treatments on CTCs and to ensure that therapies aimed at tumor-cell growth or invasion do not inadvertently increase metastatic risk.

Due to their importance in cancer progression, CTCs are being extensively studied [219], [220], [239], but primarily to count them so as to gauge patient prognosis [240], or to analyze static changes in protein [241] or gene expression [242], [243], rather than to understand CTC dynamic behavior. Antibody recognition of cell surface markers has been used to purify CTCs from blood samples that can contain as few as one CTC per billion blood cells [244]. However, these antibody-based approaches require lengthy procedures or cell fixations that prevent the observation of live CTCs. Microfluidic devices [242], [245], [246] and microfilters [247], [248] are increasing the speed of CTC isolation but remain limited in their ability to accurately manipulate detached CTCs. Suction of CTCs onto micropipettes [249], [250] or capture with optical laser traps [251]–[253] allows analysis of the mechanical properties of CTCs, but also deforms their cell surfaces and can disrupt the natural behavior of the microtentacles.

Our current aim is to manipulate detached CTCs in a contact-free manner without disturbing their McTNs so that unperturbed microtentacle behavior can be observed. CTCs are $\sim 20 \mu\text{m}$ in diameter [and up to $\sim 40 \mu\text{m}$ with extended McTNs; see Figure 12(b)] and thus are larger than the previous cells that were manipulated. They therefore required fabrication of new devices with taller $50 \mu\text{m}$ channels. Larger channels increase the velocity of disturbing flows created by surface tension pressure imbalances and make feedback control more difficult. These imbalances were removed by plugging the reservoirs with gels to eliminate the water/air menisci that created the surface tension pressures. Using EP actuation with low $< 100 \text{ V/m}$ electric fields, Figure 13 shows an initial result for steering a free-floating human MDA-436 breast tumor cell into another MDA-436 cell that has adhered to the chip surface and whose microtentacles are visible. Although microtentacles have not yet been crisply visualized in this experiment [as done by green protein fluorescent imaging in Figure 12(b)], it was clear that the two cells connected one with another and that the adhered cell held onto the floating cell until EP control was able to separate them [see Figure 13(c) and the movie].

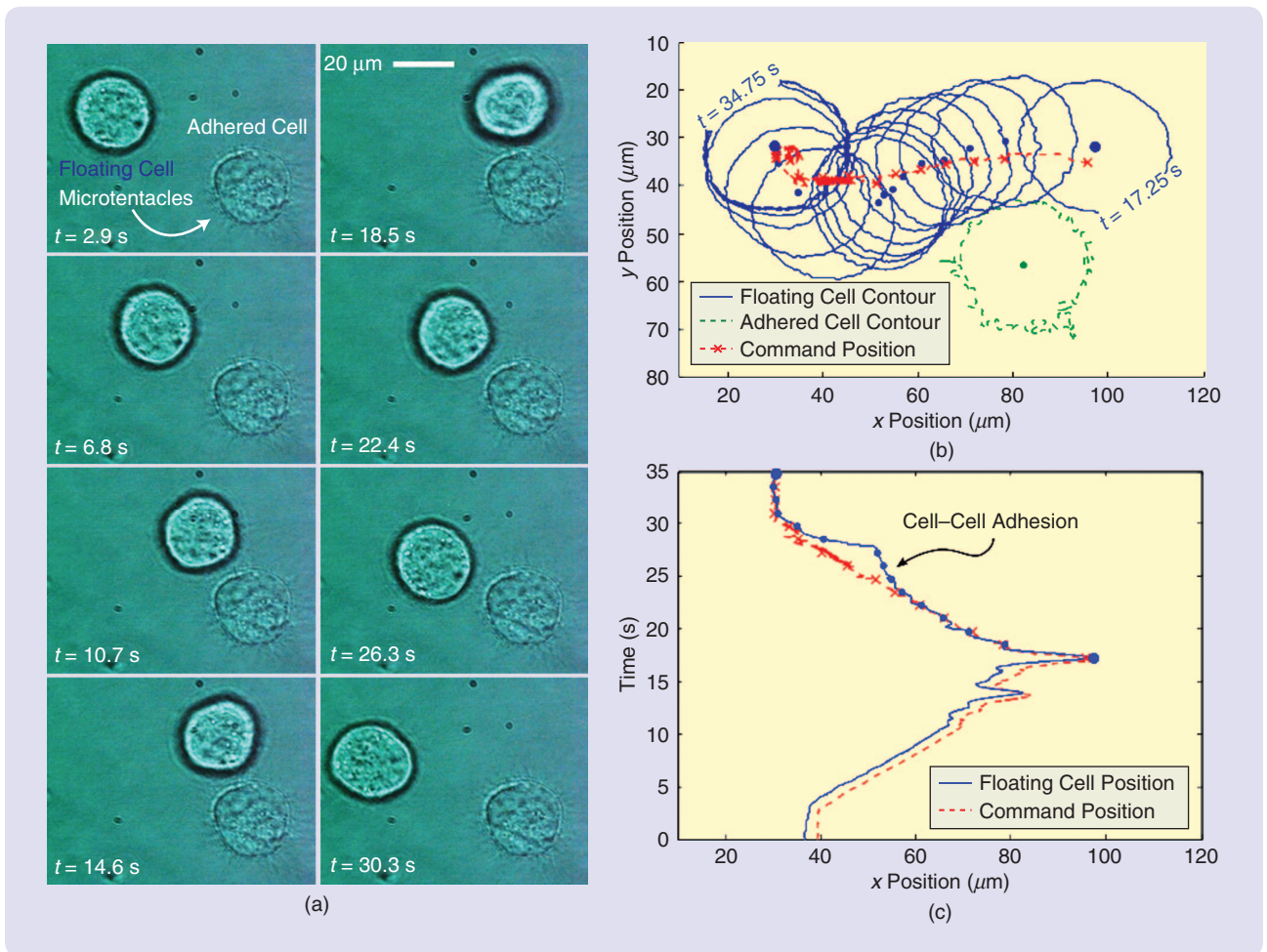


FIGURE 13 Control of a single free-floating human breast tumor MDA-MB-436 cell. (a) The cell was steered toward and away from another breast tumor cell that had adhered to the chip surface and whose microtentacles are visible as faint white extensions. (b) The trajectory of the floating cell as it is pulled away to the left from the adhered cell (during $t = 17.25$ s to 34.75 s). The commanded centroid position is shown by red crosses while the measured path and cell boundary is shown by blue dots and curves. The boundary of the adhered cell is shown in dashed green lines. (c) The x-location of the floating cell during inward and outward motion (commanded = red dashed; measured = blue solid). When the cell is pulled back, cell-to-cell adhesion retards leftward motion until the applied control breaks the two cells apart, as is clearly evident in the movie at www.controlofmicrobio.umd.edu/movies/cell-wMCTNs.mov.

The next goal is to hold CTCs in place while injecting various types of drugs into the device to test the response of MCTNs to a library of cancer drugs. Feedback control will also be used to bring floating CTCs close to one another, with and without drugs, to investigate when and how they use MCTNs to attach to each other and begin to form agglomerates. Such CTC aggregates have been observed in cancer patient blood samples [246] and predict poor patient prognosis. Animal experiments have shown that these CTC aggregates are the initial source of metastatic tumor outgrowths in lung capillary vessels rather than single CTCs which simply exit these vessels [254]. Systems to steer detached CTCs, one to another, so that aggregation can be monitored will facilitate research aimed at defining the underlying mechanisms and identifying therapeutic opportunities to disrupt this stage of tumor metastasis.

Since MCTNs promote CTC aggregation [232], [235], [255] as well as endothelial attachment [256], they are both a likely mechanism of cancer growth and a potential therapeutic target. Feedback flow or EP control provides a method to gently trap and steer floating CTCs, without disrupting their membrane mechanics, so that their natural behavior can be monitored under a microscope for sufficiently long times to collect statistically significant data.

Manipulating Nanoscopic QDs to Nanoscale Precision

The next application is manipulating nanoscopic objects to nanoscale precision. Both new features present difficulties: it is harder to manipulate more precisely *and* it is harder to manipulate smaller objects. The first challenge is that Brownian motion scales inversely with particle size—smaller particles diffuse faster [117], [195], hence, they move further

Manipulation and fluid solidification allowed sequential, high-precision positioning and immobilization of multiple individually selected nanoparticles on a two-dimensional surface.

away between control updates, making precision control more difficult. Second, most prior particle manipulation techniques, such as optical tweezers [18], [19], [82]–[84], DEP [94], [98], [257], and magnetic tweezers [30], [258] (see Table 1), create forces that scale with particle volume. Therefore, a nanometer diameter particle experiences forces that are a billion times smaller than a micrometer particle of the same material. Manipulation of nanoscopic particles thus requires either advantageous particle materials (electrical permittivity significantly exceeds that of the surrounding fluid for DEP [97]) or strong actuation (powerful magnets [258] or high powered lasers [18], [83], [84]). Even under strong actuation, the larger Brownian motion can cause nanoparticles to escape the energy traps created by optical and DEP means [40], [97]. Third, it is difficult to precisely see the location of nanoscale particles. The wavelength of light ($\lambda \sim 0.5 \mu\text{m}$) sets the minimum length scale that can be optically distinguished. Emitting nanoparticles show up as spread-out microscale diffraction patterns under the microscope—a sample diffraction pattern is shown in the top right inset of Figure 15(a)—and it is difficult to infer their precise position.

However, control of nano objects to nanometer accuracy is desirable, for example, for nanophotonic and nanoelectronic applications where there is a need to place quantum dots and nanowires in the high electric field regions of photonic [259]–[261] and plasmonic [262], [263] structures. These high field regions are approximately 150 nm in size [264], necessitating the manipulation of dots and wires to submicron accuracies. EO flow control manipulates particles by fluid drag forces that scale more favorably (with particle radius [116], [117] rather than volume) and has enabled nanoprecise manipulation of single QDs [71], [72]—a capability that has not been demonstrated by any other means.

During closed-loop particle flow control, the positioning error is determined by the sum of the vision-sensing error and the diffusion of the particle between control updates [72]. Other errors, such as flow actuation misalignments and mechanical vibrations, are smaller. For the previ-

ous cell and bead control, the manipulation precision was limited by the $1 \mu\text{m}$ accuracy of the vision sensing [68]. This imaging accuracy was a consequence of the hardware used ($1 \mu\text{m}$ in the device corresponded to one pixel in the camera image), but it also approached the fundamental wavelength-of-light limitation. It is possible, however, to significantly improve vision sensing beyond the wavelength of light. The key is to realize that the visible diffraction spot for a nanoscopic particle, such as a QD, can span many camera pixels. By averaging correctly over these pixels, it is possible to infer the center of the diffraction pattern to better than single pixel resolution, a technique known as subpixel averaging [265]. If a Gaussian pattern is fitted to the diffraction spot shown in the inset of Figure 15(a), the centroid of that Gaussian is inferred to better than the width of a single pixel. Subpixel averaging is implemented below in real time, and, together with particle dynamics and feedback control (which still obey the same governing equations as before), enables control of single QDs to nanoscale precision.

Figure 14 shows the hardware and control loops for flow control of a single QD [72]. The QDs used were elliptical in shape and had a size of 6 nm on the major and 3 nm on the minor axis. In addition to strong Brownian motion and

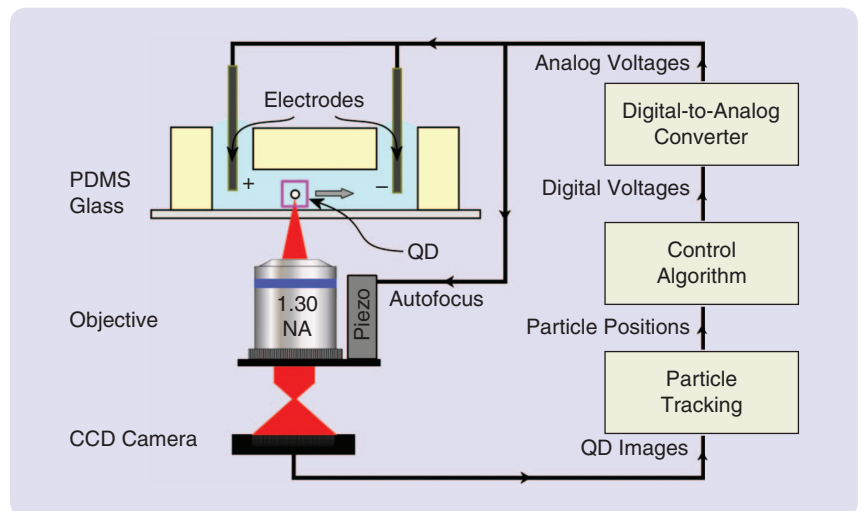


FIGURE 14 The experimental setup and control loops for manipulation of a single quantum dot (QD) to nanoscale precision. A charge-coupled device (CCD) camera images the QD and sends the information to a tracking algorithm that uses sub-pixel averaging to accurately determine the current position of the QD to 19 nm precision. The control algorithm uses this information to determine the proper voltages to apply to the electrodes in order to move the QD to its desired position. A second feedback loop moves the imaging objective in the z direction using a piezo stage to keep the QD in focus [72].

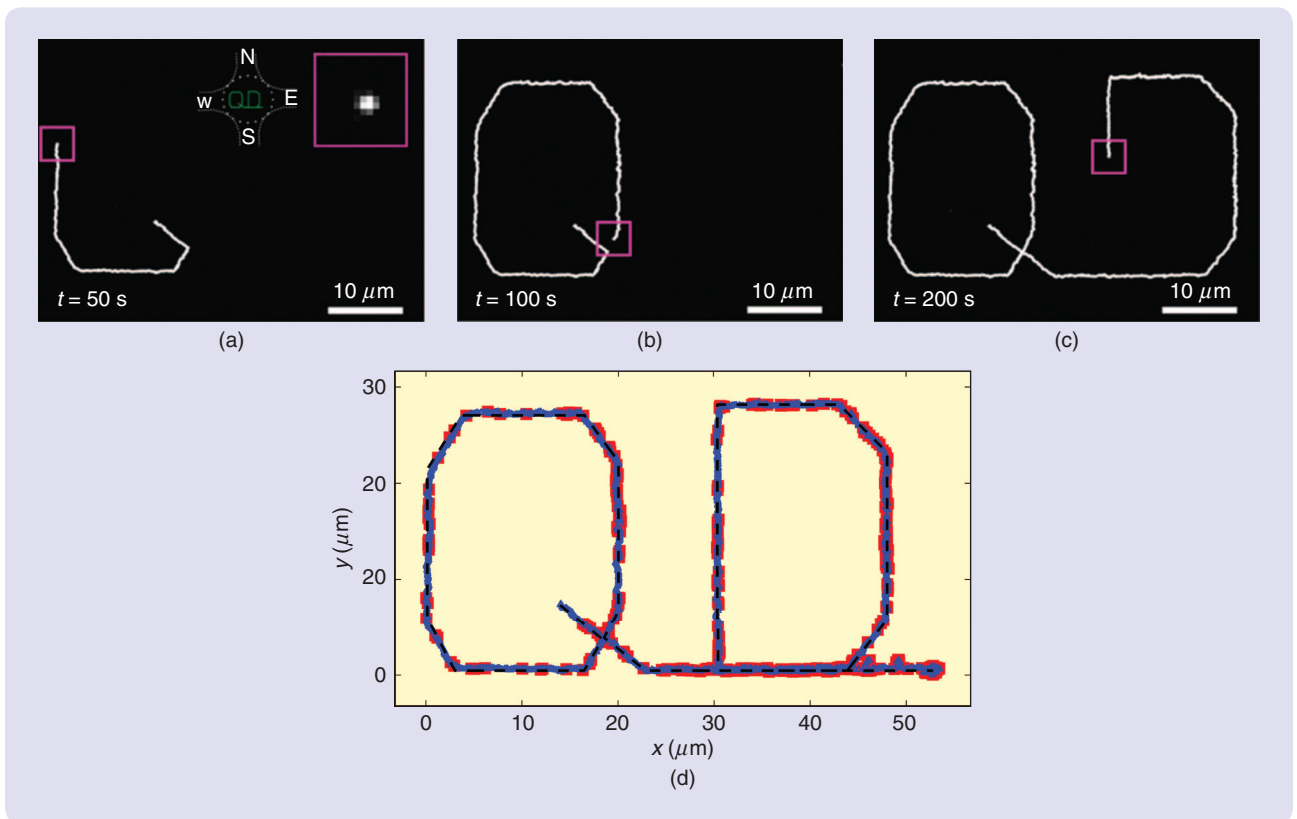


FIGURE 15 Flow control of a single quantum dot (QD) to nanoscale precision [72]. Panels (a)–(c) show charge-coupled device (CCD) camera images of the QD being steered along the desired trajectory (www.controlofmicrobio.umd.edu/movies/QD.mov). The white trace shows the measured path of the QD up until its current location. In panel (a), the magenta box inset shows the subpixel averaging window and the image of the QD diffraction pattern it contains. The second inset shows the orientation of the QD trajectory (green) with respect to the four electrodes. Panel (d) traces a plot of QD position along its trajectory. The underlying dotted black line shows the desired trajectory, blue represents the actual measured QD trajectory, and the solid red squares depict when the QD blinks off. The mean displacement from the trajectory is calculated to be 119.5 nm. At the end of the trajectory, the QD is held in place for 2 min (not shown in the online movie).

large diffraction patterns, which present problems for nanoprecise control of all nanoscopic objects, QDs also present additional issues. QDs blink on and off, and the control does not know where they are when they blink out of view. To handle this issue, the control is paused when the QD blinks off and is resumed when it begins to re-emit. Together with localized fluid solidification (discussed next) this strategy still allows point-to-point placement and immobilization of specific dots on chip.

QD position is controlled in the horizontal plane but the QD still diffuses in the vertical direction. This diffusion makes the QD leave the focal plane of the microscope and causes a defocusing that hurts the subpixel sensing accuracy. A second control loop uses the variance of the QD image as its metric and drives this metric to a minimum by moving the microscope objective up or down using a piezo stage. Since being above or below the objective focal plane defocuses the image in the same way, this second loop introduces a small vertical jitter to determine if the dot looks more focused when moving an additional amount up or down. This jitter provides information on

whether the dot is above or below the focal plane of the microscope and a Newton-bracketing algorithm is then used to control to the minimum image variance. The inner loop runs slowly compared to the outer horizontal positioning loop, since out-of-focus drift is a slower process, and it enables higher accuracy QD manipulation in the horizontal plane.

In addition to subpixel averaging, pausing for blinking, and vertical focus tracking, the chemistry of the buffer had to be carefully chosen to meet QD control requirements. The fluid had to exhibit electroosmosis and not damage the PDMS material of the microfluid devices. It also had to have a high viscosity to decrease QD Brownian motion, which is a key source of positioning error. Finally, the buffer chemistry had to be compatible with the QDs; they had to remain suspended as single dots and not aggregate into clumps. Water with an added associating polymer (to increase the fluid viscosity) and a zwitterionic betaine surfactant (to retain effective EO actuation) was chosen as the buffer fluid [72] based on input from the team chemists (J. Fourkas and S. Raghavan) as well as by

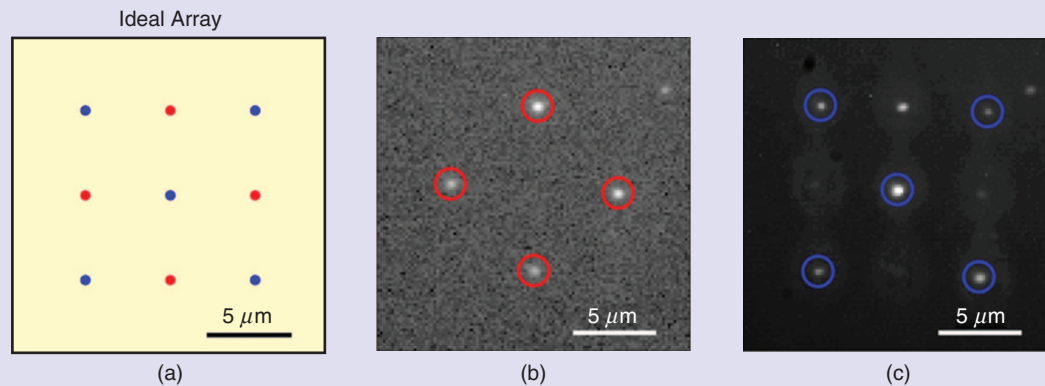


FIGURE 16 Electroosmotic flow control and immobilization of two types of quantum dots (QDs) on a chip surface [71]. (a) Desired array with the two types of QDs alternating in a checkerboard pattern. (b) Completed array as visualized through a bandpass filter centered at a 710-nm wavelength. The four QDs emitting at ~ 705 nm are circled in red, the 655 nm emitting QDs are not visible. (c) The same completed array as visualized through the 65-nm band pass filter. The QDs emitting at 655 nm are circled in blue.

extended and systematic trial and error. This buffer choice yielded EO flow actuation along with high viscosity and singly dispersed QDs.

In the experiments, flow control could hold a single QD to a target location with 45 nm accuracy and, as shown in Figure 15, could steer it along a chosen path with a mean deviation of 120 nm [72]. The 6 nm sized dot could be controlled for one hour, its usable (visible) lifetime. The precision of the vision sensing was determined by monitoring the measured centroid location of a stationary QD adhered to a glass slide. These measurements had a standard deviation of 19 nm. Subtracting this 19 nm vision noise from the observed deviation of the controlled QD yielded the 45 nm (when trapped) and 120 nm (when steered) accuracies.

For fabrication of multidot quantum information systems, it is not enough to control the QD to the correct location in a fluid. The QD must be delivered to the surface of the photonic chip, must be fixed in place, and then the next QD must be brought into place and attached to the chip. To have a QD couple to a photonic cavity, this must be done to nanoscale precision—the QD should be placed within the ~ 150 nm wide high-mode region of the cavity [264]. An appropriate modification of fluid chemistry neatly solved all these issues. To confine QDs to the chip surface, a low-viscosity, water-based, negative-tone photoresist was used. (A photoresist is a light-sensitive polymer that cross-links and solidifies the fluid under strong light, allowing QD immobilization.) The chemical properties of this photoresist caused the QDs to segregate to the surfaces (ceiling, walls, and chip surface floor) of the microfluidic device [71]. The microscope focal plane was lowered to the bottom of the device to keep QDs on the chip surface in focus, and EO flow control was used to move a chosen QD to its target location. Once a QD was in place, a brief ultraviolet laser

pulse polymerized a small cap of fluid immediately around the positioned QD to permanently fix it in place on the chip surface. This small solid region did not affect the manipulation of subsequent QDs. Manipulation and fluid solidification allowed sequential, high-precision positioning and immobilization of multiple individually selected nanoparticles on a two-dimensional surface. Figure 16 shows the placement and fixing of two different types of QDs in a grid on the chip surface, to 127-nm precision [71]. These single QDs remained in place and continued emitting even after the flow control microfluidic device was peeled off.

CONCLUSION

Modeling and feedback control has enabled simple PDMS-on-glass devices, which can be fabricated in under an hour, to manipulate a variety of cells including bacteria, animal cells, and live human cells to single micron precision. EK control has neither harmed robust river micro-organisms nor fragile live human cells. Cells have been manipulated in a variety of fluids: in cell media, river water, in a liposome buffer (a liquid containing micelles with fluorescent dyes to mark specific cell types), and in diluted blood. Least-squares algorithms have allowed independent manipulation of a small number of cells simultaneously, which is useful for cell-to-cell studies. The same least-squares algorithms are also enabling 3D [215] and rotational [76] control.

Gentle EK cell control is well suited to the manipulation of live human cells without disturbing their activity and therefore is being used to study the microtentacled behavior of live human cancer cells. EK feedback control has also been used to manipulate nanoscopic particles (QDs) to nanoscale precision [72]. Here the fluid chemistry was engineered to push the QDs to the chip surface and to permit local solidification of the fluid and, hence,

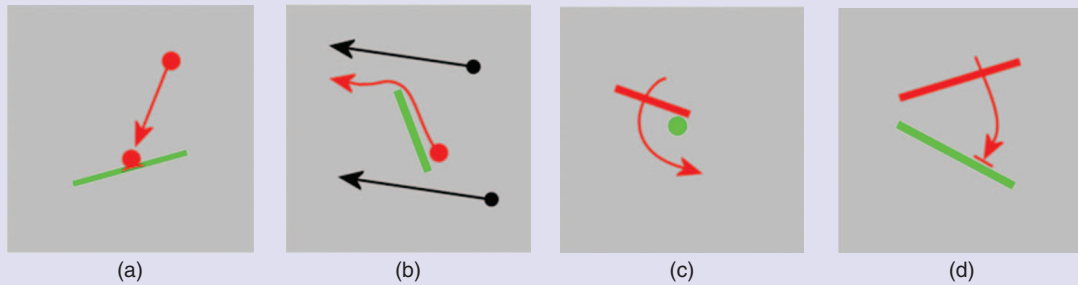


FIGURE 17 Flow control with particles and wires restricted to the chip surface and acting as guides, pivots, and constraints. Using the same experimental setup as in Figure 16, it is possible to attach particles to wires, use wires as constraints for particle motion, use particles as pivots for wires, and use wires as constraints for each other. Green shows the constraints, red shows constrained motion, and black is the motion of other unconstrained objects. Exploiting these types of constrained behaviors could enable fast and accurate snap-to assembly of micro and nanoscale components on chip. (Movies available online at www.controlofmicrobio.umd.edu/movies/QD-to-wire.mov, www.controlofmicrobio.umd.edu/movies/QD-along-wire.mov, www.controlofmicrobio.umd.edu/movies/pivot-wire.mov, and www.controlofmicrobio.umd.edu/movies/wire-to-wire.mov.) (a) Controlled immobilization, (b) constrained steering, (c) pivot with obstacle, and (d) alignment with obstacle.

immobilization of each QD after placement [71], a technique that is being used to fabricate multidot photonic systems. No alternate methods to place specific QDs to specific locations on chip have been previously demonstrated, so, in this instance, feedback flow control has enabled an entirely new capability.

The above results were enabled by physics-based modeling and simple control algorithms. Modeling of EO flow and EP forces is standard [122], [123], [143] and is sufficient for controlling nanoparticles to nanoscale precision. However, parameters in the model (surface and particle charge, viscosity, parasitic pressure flows) vary significantly. To limit key uncertainties it has been crucial to first optimize the devices (for example, by making reservoirs larger to reduce meniscus curvature and hence decrease the parasitic pressure flows created by surface tension) before using feedback to correct for the remaining errors. So far, appropriately chosen simple control designs have sufficed—except for the QD-focusing inner loop (Figure 14) all the control has been simple least squares. System performance limits have been set by device design and imaging accuracy, not so much by the type of control algorithms chosen. Now that devices and optics have been optimized, next-generation tasks such as controlling the shape of DNA strands will likely require and benefit from more sophisticated control algorithms.

The next applications for flow control are being chosen to fit the strengths of the technique. EK control has turned out to be ideally suited for the manipulation of live suspended human cancer cells and nanophotonic objects. Unlike laser tweezers, EK manipulation does not create a strong optical trap for each cell that can deform its shape and disturb microtentacle behavior [251]–[253]. Also compared to laser tweezers, EK control enables manipulation

of nanoscopic objects to nanoscale precision on chip regardless of their material properties (see Table 1). For the manipulation and observation of live tentacled cancer cells, the next steps are to adapt the device designs so that cancer drugs can be injected into the cell chambers without disrupting flow control and to extend the control algorithms to allow better cell-to-cell manipulation to study microtentacle interlocking during cell-to-cell adhesion. As mentioned in the discussion surrounding Figure 10, the latter task is being achieved by modifying the control algorithm to reduce the distance between two cells (one degree of freedom control) rather than steer both cells along a specified trajectory (more highly constrained four degrees of freedom control).

For nanophotonic applications, fluid and object chemistry plays a crucial role. Figure 16 shows one result for control of QDs that are confined to the chip surface by a QD-exclusion fluid chemistry (the low-viscosity, water-based, negative-tone photoresist). Figure 17 further illustrates how confinement of wires and particles to the chip surface can enable useful new motion primitives. By varying chemistry globally or locally by laser pulses, it is possible to stick dots to wires, use wires as constraints for QD motion, use particles as pivots for wire rotation, and to quickly align one wire with another. Using nanoscopic objects as constraints for each other raises interesting optimal path planning issues, such as what combination of translation/rotation flow control [76] and particle/wire pivots should be used to most quickly assemble multiobject nanophotonic components. Thus there is a need to understand how to optimally meld flow control with chemically modulated chip-surface motion constraints.

More broadly, flow control is part of a complex landscape for manipulating microscopic and nanoscopic

Most importantly, feedback control of micro/nano systems for electronic and biological applications requires a tight collaboration between control theorists and domain experts in micro- and nanoscale science, biology, and medicine.

objects (see Table 1). This article has focused on modeling and control methods for EK control, which includes both EO flow control and EP control of objects that acquire surface charge, but the same general approach (vision sensing, modeling-for-control, and simple algorithms that reliably invert maps from actuation to motion) can likely be used to improve on-chip control by DEP, optoelectronic, acoustic, and other actuation means. In addition to EK actuation, feedback control is already being applied to magnetic tweezers [62], [108], [110]–[112] and DEP manipulation [37], [42], [43], but there remain strong opportunities for feedback control in acoustic and optoelectronic devices.

There is also a strong need for system integration. In a cancer patient's blood, as few as one out of a billion cells are circulating tumor cells; no single actuation modality will be able to reliably extract, keep alive, and then study such rare cells from blood samples. Instead, an integrated system with multiple types of sensing and actuation is required, and feedback control will be essential to enable such systems. For microscale applications, as on the macroscale, feedback can dramatically improve performance and system robustness, but it requires modeling for control as well as effective real-time sensing, translation of application needs into tractable control formulations, real-time control algorithms, system integration, and experimental verification. Most importantly, feedback control of micro/nano systems for electronic and biological applications requires a tight collaboration between control theorists and domain experts in micro- and nanoscale science, biology, and medicine. Our hope is that this article has illustrated some interesting application opportunities and will perhaps inspire future efforts and collaborations.

ACKNOWLEDGMENTS

A large number of students, post-docs, and collaborators have made this research possible. The help of Mike Armani, Rodica Bauer, Andrew Berglund, Satej Chaudhary, John Fourkas, Barbara Gerratana, Rakesh Kumar, Alex Liddle, Pramod Mathai, Stuart Martin, Tamara McNealy, Silvia Muro, Alek Nacev, Sijia Qin, Srinivasa Raghavan, Sina Sahand, Shawn Walker, and Ian White is greatly appreciated. Funding support was provided by the NSF and DARPA and is gratefully acknowledged.

AUTHOR INFORMATION

Roland Probst received a diploma in computer engineering from the University of Applied Sciences, Mannheim, Germany, and a Ph.D. in aerospace engineering from the University of Maryland, College Park. He is currently a research associate with the Fischell Department of Bioengineering at the University of Maryland. His main interest is to create innovative methods to facilitate control of micro and nanoscaled systems by EK and magnetic actuation. He currently is developing 3D EK tweezers for nanoassembly applications.

Zachary Cummins received a B.S. degree in aerospace engineering at the University of Maryland in 2009 and is currently pursuing his Ph.D. in the Fischell Department of Bioengineering. His research interests include the design and control of microfluidic systems, especially to optimize techniques for precise and tractable handling of microorganisms.

Chad Ropp received a B.S. degree in electrical and computer engineering from the University of Maryland in 2007 and is currently working toward a Ph.D. degree at the same institution. His research interests include the manipulation and assembly of colloidal nanoparticles for quantum optics and plasmonic systems.

Edo Waks received a B.Sc. and M.Sc. in electrical engineering from Johns Hopkins University and a Ph.D. in electrical engineering from Stanford University. He is an assistant professor in the Department of Electrical and Computer Engineering at the University of Maryland, College Park, and is also a member of the Institute for Research in Electronics and Applied Physics and the Joint Quantum Institute. His research is in the area of semiconductor nanophotonics, nonlinear optics, and quantum optics, where he focuses on the properties of quantum emitters coupled to nanoscale photonic structures.

Benjamin Shapiro (benshap@umd.edu) received a B.S. in aerospace engineering from the Georgia Institute of Technology and a Ph.D. in the control and dynamical systems option at the California Institute of Technology where he worked on symmetry breaking in jet engines. He joined the Department of Aerospace Engineering at the University of Maryland in 2000. His interests at Maryland have shifted to the control of miniaturized systems, with a focus on systems for biomedical applications. In 2009, he spent his sabbatical at NIH and

NIST, half of the time within the Advanced Technology Center at the National Cancer Institute, the other half at the Center for Nanoscale Science and Technology at the National Institute of Standards and Technology. He is currently an associate professor in the Fischell Department of Bioengineering and the Institute for Systems Research at the University of Maryland. He is also a Fulbright scholar (Germany, 2009). He can be contacted at the Fischell Department of Bioengineering, 1226 Kim Building, University of Maryland, College Park, MD 20742 USA.

REFERENCES

- [1] S. R. Quake and T. M. Squires, "Microfluidics: Fluid physics at the nanoliter scale," *Rev. Modern Phys.*, vol. 77, no. 3, pp. 977–1026, 2005.
- [2] G. M. Whitesides, "The origins and the future of microfluidics," *Nature*, vol. 442, pp. 368–373, July 2006.
- [3] J. C. T. Eijkel and A. v. d. Berg, "Nanofluidics: What is it and what can we expect from it?," *Microfluid. Nanofluid.*, vol. 1, pp. 249–267, Apr. 2005.
- [4] M. Napoli, J. C. T. Eijkel, and S. Pennathur, "Nanofluidic technology for biomolecule applications: A critical review," *Lab Chip*, vol. 10, no. 8, pp. 957–985, 2010.
- [5] D. Figeys, "Adapting arrays and lab-on-a-chip technology for proteomics," *Proteomics*, vol. 2, no. 4, pp. 373–382, 2002.
- [6] R. Jabeen, D. Payne, J. Wiktorowicz, A. Mohammad, and J. Petersen, "Capillary electrophoresis and the clinical laboratory," *Electrophoresis*, vol. 27, no. 12, pp. 2413–2438, 2006.
- [7] M. A. Northrup, B. Benett, D. Hadley, P. Landre, S. Lehew, J. Richards, and P. Stratton, "A miniature analytical instrument for nucleic acids based on micromachined silicon reaction chambers," *Anal. Chem.*, vol. 70, no. 5, pp. 918–922, 1998.
- [8] J. El-Ali, P. K. Sorger, and K. F. Jensen, "Cells on chips," *Nature*, vol. 442, no. 27, pp. 403–411, 2006.
- [9] G. Spera, "Implantable pumps improve drug delivery, strengthen weak hearts," *Med. Dev. Diagn. Indust. Mag.*, vol. 19, p. 59, 1997.
- [10] E. A. Ottesen, J. W. Hong, S. R. Quake, and J. R. Leadbetter, "Microfluidic digital PCR enables multigene analysis of individual environmental bacteria," *Science*, vol. 314, pp. 1464–1467, Dec. 2006.
- [11] J. Fu, R. B. Schoch, A. L. Stevens, S. R. Tannenbaum, and J. Han, "A patterned anisotropic nanofluidic sieving structure for continuous-flow separation of DNA and proteins," *Nat. Nanotechnol.*, vol. 2, pp. 121–128, Feb. 2007.
- [12] R. Fan, O. Vermesh, A. Srivastava, B. K. H. Yen, L. Qin, H. Ahmad, G. A. Kwong, C. Liu, J. Gould, L. Hood, and J. R. Heath, "Integrated barcode chips for rapid, multiplexed analysis of proteins in microliter quantities of blood," *Nat. Biotech.*, vol. 26, pp. 1373–1378, Dec. 2008.
- [13] D. Wu and A. J. Steckl, "High speed nanofluidic protein accumulator," *Lab Chip*, vol. 9, no. 13, pp. 1890–1896, 2009.
- [14] P. J. Lee, P. J. Hung, R. Shaw, L. Jan, and L. P. Lee, "Microfluidic application-specific integrated device for monitoring direct cell-cell communication via gap junctions between individual cell pairs," *Appl. Phys. Lett.*, vol. 86, no. 22, pp. 223902–223905, 2005.
- [15] K. Terao, Y. Kitazawa, R. Yokokawa, A. Okonogi, and H. Kotera, "Open-access and multi-directional electroosmotic flow chip for positioning heterotypic cells," *Lab Chip*, vol. 11, no. 8, pp. 1507–1512, 2011.
- [16] P. S. Dittich and A. Manz, "Lab-on-a-chip: Microfluidics in drug discovery," *Nat. Rev. Drug Discov.*, vol. 5, pp. 210–218, Mar. 2006.
- [17] S. Sugiura, K. Hattori, and T. Kanamori, "Microfluidic serial dilution cell-based assay for analyzing drug dose response over a wide concentration range," *Anal. Chem.*, vol. 82, pp. 8278–8282, Oct. 2010.
- [18] D. G. Grier, "A revolution in optical manipulation," *Nat. Photon.*, vol. 424, no. 6950, pp. 810–816, 2003.
- [19] J. E. Curtis, B. A. Koss, and D. G. Grier, "Dynamic holographic optical tweezers," *Opt. Commun.*, vol. 207, no. 1–6, pp. 169–175, 2002.
- [20] H. Zhang and K. Liu, "Optical tweezers for single cells," *J. Roy. Soc., Interface Roy. Soc.*, vol. 5, pp. 671–690, July 2008.
- [21] A. Ashkin, J. M. Dziedzic, and T. Yamane, "Optical trapping and manipulation of single cells using infrared laser beams," *Nature*, vol. 330, no. 6150, pp. 769–771, Dec. 1987.
- [22] Y. Tanaka, H. Kawada, K. Hirano, M. Ishikawa, and H. Kitajima, "Automated manipulation of non-spherical micro-objects using optical tweezers combined with image processing techniques," *Opt. Express*, vol. 16, no. 19, pp. 15115–15122, 2008.
- [23] F. Arai, T. Sakami, K. Yoshikawa, H. Maruyama, and T. Fukuda, "Synchronized laser micromanipulation of microtools for assembly of microbeads and indirect manipulation of microbe," in *Proc. IEEE/RSJ Int. Conf. Intelligent Robots and Systems (IROS)*, Oct. 2003, vol. 3, pp. 2121–2126.
- [24] S. Ito, H. Yoshikawa, and H. Masuhara, "Laser manipulation and fixation of single gold nanoparticles in solution at room temperature," *Appl. Phys. Lett.*, vol. 80, no. 3, pp. 482–485, 2002.
- [25] F. Hajizadeh and S. S. Reihani, "Optimized optical trapping of gold nanoparticles," *Opt. Express*, vol. 18, pp. 551–559, Jan. 2010.
- [26] R. Agarwal, K. Ladavac, Y. Roichman, G. Yu, C. Lieber, and D. Grier, "Manipulation and assembly of nanowires with holographic optical traps," *Opt. Express*, vol. 13, pp. 8906–8912, Oct. 2005.
- [27] H. Maruyama, K. Kotani, T. Masuda, A. Honda, T. Takahata, and F. Arai, "Nanomanipulation of single influenza virus using dielectrophoretic concentration and optical tweezers for single virus infection to a specific cell on a microfluidic chip," *Microfluid. Nanofluid.*, vol. 10, pp. 1109–1117, Dec. 2010.
- [28] F. Arai, T. Endo, R. Yamuchi, and T. Fukuda, "3D 6DOF manipulation of micro-object using laser trapped microtool," in *Proc. IEEE Int. Conf. Robotics and Automation, ICRA*, May 2006, pp. 1390–1395.
- [29] A. E. Wallin, H. Ojala, G. Ziedaite, and E. Haggstroem, "Dual-trap optical tweezers with real-time force clamp control," *Rev. Scientif. Instrum.*, vol. 82, no. 8, pp. 083102–083109, 2011.
- [30] K. C. Neuman and A. Nagy, "Single-molecule force spectroscopy: Optical tweezers, magnetic tweezers and atomic force microscopy," *Nat. Meth.*, vol. 5, pp. 491–505, June 2008.
- [31] V. Bingelyte, J. Leach, J. Courtial, and M. J. Padgett, "Optically controlled three-dimensional rotation of microscopic objects," *Appl. Phys. Lett.*, vol. 82, no. 5, pp. 829–831, 2003.
- [32] M. K. Kreysing, T. Kiehling, A. Fritsch, C. Dietrich, J. R. Guck, and J. A. Kaes, "The optical cell rotator," *Opt. Express*, vol. 16, pp. 16984–16992, Oct. 2008.
- [33] R. S. Thomas, H. Morgan, and N. G. Green, "Negative DEP traps for single cell immobilisation," *Lab Chip*, vol. 9, no. 11, pp. 1534–1540, 2009.
- [34] J. Huang, G. Wang, K. Tseng, and S. Fang, "A chip for catching, separating, and transporting bio-particles with dielectrophoresis," *J. Indust. Microbiol. Biotechnol.*, vol. 35, pp. 1551–1557, Nov. 2008.
- [35] H. Morgan, T. Sun, D. Holmes, S. Gawad, and N. G. Green, "Single cell dielectric spectroscopy," *J. Phys. D: Appl. Phys.*, vol. 40, no. 1, pp. 61–70, 2007.
- [36] T. Hunt and R. Westervelt, "Dielectrophoresis tweezers for single cell manipulation," *Biomed. Microdev.*, vol. 8, no. 3, pp. 227–230, 2006.
- [37] B. Edwards, N. Engheta, and S. Evoy, "Electric tweezers: Experimental study of positive dielectrophoresis-based positioning and orientation of a nanorod," *J. Appl. Phys.*, vol. 102, pp. 024913–5, July 2007.
- [38] B. H. Lapizco-Encinas and M. Rito-Palomares, "Dielectrophoresis for the manipulation of nanobioparticles," *Electrophoresis*, vol. 28, no. 24, pp. 4521–4538, 2007.
- [39] C. Zhang, K. Khoshmanesh, A. Mitchell, and K. Kalantar-zadeh, "Dielectrophoresis for manipulation of micro/nano particles in microfluidic systems," *Anal. Bioanal. Chem.*, vol. 396, pp. 401–420, July 2009.
- [40] R. Hoelzel, N. Calander, Z. Chiragwandi, M. Willander, and F. F. Bier, "Trapping single molecules by dielectrophoresis," *Phys. Rev. Lett.*, vol. 95, pp. 128102–128106, Sept. 2005.
- [41] J. Voldman, R. A. Braff, M. Toner, M. L. Gray, and M. A. Schmidt, "Holding forces of single-particle dielectrophoretic traps," *Biophys. J.*, vol. 80, pp. 531–542, Jan. 2001.
- [42] D. E. Chang and N. Petit, "Toward controlling dielectrophoresis," *Int. J. Robust Nonlinear Contr.*, vol. 15, no. 16, pp. 769–784, 2005.

- [43] M. P. Melnyk and D. E. Chang, "Time optimal control of a dielectrophoretic system," *Asian J. Contr.*, vol. 13, no. 4, pp. 480–491, 2006.
- [44] P. Y. Chiou, A. T. Ohta, and M. C. Wu, "Massively parallel manipulation of single cells and microparticles using optical images," *Nature*, vol. 436, pp. 370–372, July 2005.
- [45] G. J. Shah, A. T. Ohta, E. P. Chiou, M. C. Wu, and C. C. Kim, "EWOD-driven droplet microfluidic device integrated with optoelectronic tweezers as an automated platform for cellular isolation and analysis," *Lab Chip*, vol. 9, no. 12, pp. 1732–1739, 2009.
- [46] A. T. Ohta, P. Chiou, H. L. Phan, S. W. Sherwood, J. M. Yang, A. N. Lau, H. Y. Hsu, A. Jamshidi, and M. C. Wu, "Optically controlled cell discrimination and trapping using optoelectronic tweezers," *IEEE J. Select. Topics Quantum Electron.*, vol. 13, pp. 235–243, Apr. 2007.
- [47] H.-y. Hsu, A. T. Ohta, P. Chiou, A. Jamshidi, S. L. Neale, and M. C. Wu, "Phototransistor-based optoelectronic tweezers for dynamic cell manipulation in cell culture media," *Lab Chip*, vol. 10, no. 2, pp. 165–172, 2010.
- [48] A. Jamshidi, H. Hsu, J. K. Valley, A. T. Ohta, S. Neale, and M. C. Wu, "Metallic nanoparticle manipulation using optoelectronic tweezers," in *Proc. IEEE 22nd Int. Conf. Micro Electro Mechanical Systems*, Jan. 2009, pp. 579–582.
- [49] A. Jamshidi, P. J. Pauzaskie, P. J. Schuck, A. T. Ohta, P. Chiou, J. Chou, P. Yang, and M. C. Wu, "Dynamic manipulation and separation of individual semiconducting and metallic nanowires," *Nat. Photon.*, vol. 2, pp. 86–89, Feb. 2008.
- [50] J. Wu, "Acoustical tweezers," *J. Acoust. Soc. Amer.*, vol. 89, pp. 2140–2143, May 1991.
- [51] G. Barrios and R. Rechtman, "Dynamics of an acoustically levitated particle using the lattice boltzmann method," *J. Fluid Mech.*, vol. 596, pp. 191–200, 2008.
- [52] M. Saito, N. Kitamura, and M. Terauchi, "Ultrasonic manipulation of locomotive microorganisms and evaluation of their activity," *J. Appl. Phys.*, vol. 92, no. 12, pp. 7581–7587, 2002.
- [53] H. M. Hertz, "Standing-wave acoustic trap for nonintrusive positioning of microparticles," *J. Appl. Phys.*, vol. 78, no. 8, pp. 4845–4850, 1995.
- [54] J. Wang and J. Dual, "Theoretical and numerical calculations for the time-averaged acoustic force and torque acting on a rigid cylinder of arbitrary size in a low viscosity fluid," *J. Acoust. Soc. Amer.*, vol. 129, no. 6, pp. 3490–3501, 2011.
- [55] A. Haake and J. Dual, "Contactless micromanipulation of small particles by an ultrasound field excited by a vibrating body," *J. Acoust. Soc. Amer.*, vol. 117, pp. 2752–2760, May 2005.
- [56] T. Lilliehorn, M. Nilsson, U. Simu, S. Johansson, M. Almqvist, J. Nilsson, and T. Laurell, "Dynamic arraying of microbeads for bioassays in microfluidic channels," *Sens. Actuat. B: Chem.*, vol. 106, pp. 851–858, May 2005.
- [57] S. K. Chung and S. K. Cho, "3-D manipulation of millimeter- and micro-sized objects using an acoustically excited oscillating bubble," *Microfluid. Nanofluid.*, vol. 6, pp. 261–265, July 2008.
- [58] A. H. d. Vries, B. E. Krenn, R. v. Driel, and J. S. Kanger, "Micro magnetic tweezers for nanomanipulation inside live cells," *Biophys. J.*, vol. 88, pp. 2137–2144, Mar. 2005.
- [59] F. Amblard, B. Yurke, A. Pargellis, and S. Leibler, "A magnetic manipulator for studying local rheology and micromechanical properties of biological systems," *Rev. Scientif. Instrum.*, vol. 67, pp. 818–827, Mar. 1996.
- [60] J. K. Fisher, J. Cribb, K. V. Desai, L. Vicci, B. Wilde, K. Keller, R. M. Taylor, J. Haase, K. Bloom, E. T. O'Brien, and R. Superfine, "Thin foil magnetic force system for high numerical aperture microscopy," *Rev. Scientif. Instrum.*, vol. 77, no. 2, pp. 023702–023711, 2006.
- [61] C. Gosse, "Magnetic tweezers: Micromanipulation and force measurement at the molecular level," *Biophys. J.*, vol. 82, pp. 3314–3329, June 2002.
- [62] M. P. Kummer, J. J. Abbott, B. E. Kratochvil, R. Borer, A. Sengul, and B. J. Nelson, "OctoMag: An electromagnet system for 5-DOF wireless micro-manipulation," *IEEE Trans. Robot.*, vol. 26, pp. 1006–1017, Dec. 2010.
- [63] H. Lee, A. M. Purdon, and R. M. Westervelt, "Manipulation of biological cells using a microelectromagnet matrix," *Appl. Phys. Lett.*, vol. 85, no. 6, pp. 1063–1066, 2004.
- [64] H. Lee, Y. Liu, R. M. Westervelt, and D. Ham, "IC/microfluidic hybrid system for magnetic manipulation of biological cells," *IEEE J. Solid-State Circuits*, vol. 41, pp. 1471–1480, June 2006.
- [65] M. Tanyeri, M. Ranka, N. Sittipolkul, and C. M. Schroeder, "A microfluidic-based hydrodynamic trap: Design and implementation," *Lab Chip*, vol. 11, no. 10, pp. 1786–1794, 2011.
- [66] M. D. Curtis, G. J. Sheard, and A. Fouras, "Feedback control system simulator for the control of biological cells in microfluidic cross slots and integrated microfluidic systems," *Lab Chip*, vol. 11, no. 14, pp. 2343–2351, 2011.
- [67] M. Tanyeri, E. M. Johnson-Chavarria, and C. M. Schroeder, "Hydrodynamic trap for single particles and cells," *Appl. Phys. Lett.*, vol. 96, no. 22, pp. 224101–224104, 2010.
- [68] M. Armani, S. Chaudhary, R. Probst, and B. Shapiro, "Using feedback control and micro-fluidics to independently steer multiple particles," *J. Microelectromech. Syst.*, vol. 15, no. 4, pp. 945–956, 2006.
- [69] R. Probst, "Optimal control of objects on the micro- and nano-scale by electrokinetic and electromagnetic manipulation: for bio-sample preparation, quantum information devices, and magnetic drug delivery," Ph.D. dissertation, Univ. Maryland, College Park, 2010.
- [70] E. B. Steager, M. S. Sakar, D. H. Kim, V. Kumar, G. J. Pappas, and M. J. Kim, "Electrokinetic and optical control of bacterial microrobots," *J. Micro-mech. Microeng.*, vol. 21, pp. 035001–035009, Mar. 2011.
- [71] C. Ropp, Z. Cummins, R. Probst, S. Qin, J. T. Fourkas, B. Shapiro, and E. Waks, "Position and immobilization of individual quantum dots with nanoscale precision," *Nanoletters*, vol. 10, no. 11, pp. 4673–4679, 2010.
- [72] C. Ropp, R. Probst, Z. Cummins, R. Kumar, A. J. Bergland, S. R. Raghavan, E. Waks, and B. Shapiro, "Manipulating quantum dots to nanometer precision by control of flow," *Nanoletters*, vol. 10, no. 7, pp. 2525–2530, 2010.
- [73] A. E. Cohen and W. E. Moerner, "Controlling brownian motion of single protein molecules and single fluorophores in aqueous buffer," *Opt. Express*, vol. 16, pp. 6941–6956, May 2008.
- [74] A. E. Cohen and W. E. Moerner, "Method for trapping and manipulating nanoscale objects in solution," *Appl. Phys. Lett.*, vol. 86, pp. 093109–3, Feb. 2005.
- [75] A. P. Fields and A. E. Cohen, "Electrokinetic trapping at the one nanometer limit," *Proc. Nat. Acad. Sci. USA*, vol. 108, pp. 8937–8942, May 2011.
- [76] P. P. Mathai, A. J. Bergland, A. J. Little, and B. Shapiro, "Simultaneous positioning and orientation of a single nano-object by flow control," *New J. Phys.*, vol. 13, p. 013027–013054, Jan. 2011.
- [77] J. K. King, "Microfluidic device for the electrokinetic manipulation of single molecules," M.S. thesis, Univ. of Tennessee, Knoxville, TN, Aug. 2009.
- [78] P. P. Mathai, P. T. Carmichael, B. Shapiro, and A. J. Little, "Simultaneous positioning and orientation of single nano-objects using flow control," *NanoLetters*, submitted for publication.
- [79] T. M. Schneider, S. Mandre, and M. P. Brenner, "Algorithm for a microfluidic assembly line," *Phys. Rev. Lett.*, vol. 106, pp. 094503–094512, Feb. 2011.
- [80] M. Armani, S. Chaudhary, R. Probst, and B. Shapiro, "Micro flow control particle tweezers," in *Proc. uTAS*, Malmö, Sweden, 2004, pp. 26–30.
- [81] M. Armani, S. Chaudhary, R. Probst, and B. Shapiro, "Using feedback control and micro-fluidics to steer individual particles," in *Proc. 18th IEEE Int. Conf. Micro Electro Mechanical Systems*, Miami, FL, Jan. 2005, pp. 855–858.
- [82] A. Ashkin, "History of optical trapping and manipulation of small-neutral particle, atoms, and molecules," *IEEE J. Select. Topics Quant. Electron.*, vol. 6, no. 6, pp. 841–856, 2000.
- [83] K. C. Neuman and S. M. Block, "Optical trapping," *Rev. Scientif. Instrum.*, vol. 75, no. 9, pp. 2787–2809, 2004.
- [84] M. Dienerowitz, M. Mazilu, and K. Dholakia, "Optical manipulation of nanoparticles: A review," *J. Nanophoton.*, vol. 2, no. 1, pp. 021875–021907, 2008.
- [85] M. Padgett and R. Bowman, "Tweezers with a twist," *Nat. Photon.*, vol. 5, pp. 343–348, June 2011.
- [86] J. Leach, G. Sinclair, P. Jordan, J. Courtial, M. Padgett, J. Cooper, and Z. Laczik, "3D manipulation of particles into crystal structures using holographic optical tweezers," *Opt. Express*, vol. 12, pp. 220–226, Jan. 2004.

- [87] D. B. Conkey, R. P. Trivedi, S. R. P. Pavani, I. I. Smalyukh, and R. Piestun, "Three-dimensional parallel particle manipulation and tracking by integrating holographic optical tweezers and engineered point spread functions," *Opt. Express*, vol. 19, pp. 3835–3842, Feb. 2011.
- [88] G. Thalhammer, R. Steiger, S. Bernet, and M. Ritsch-Marte, "Optical macro-tweezers: Trapping of highly motile micro-organisms," *J. Opt.*, vol. 13, pp. 4024–4030, Apr. 2011.
- [89] S. Chu, "The manipulation of neutral particles," *Rev. Modern Phys.*, vol. 70, no. 3, pp. 685–706, 1998.
- [90] E. A. Cornell and C. E. Wieman, "Nobel lecture: Bose-Einstein condensation in a dilute gas, the first 70 years and some recent experiments," *Rev. Modern Phys.*, vol. 74, no. 3, pp. 875–893, 2002.
- [91] J. Beugnon, C. Tuchendler, H. Marion, A. Gaetan, Y. Miroshnychenko, Y. R. P. Sortais, A. M. Lance, M. P. A. Jones, G. Messin, A. Browaeys, and P. Grangier, "Two-dimensional transport and transfer of a single atomic qubit in optical tweezers," *Nat. Phys.*, vol. 3, pp. 696–699, Oct. 2007.
- [92] A. Kubanek, M. Koch, C. Sames, A. Ourjoumtsev, P. W. H. Pinkse, K. Murr, and G. Rempe, "Photon-by-photon feedback control of a single-atom trajectory," *Nature*, vol. 462, pp. 898–901, Dec. 2009.
- [93] T. Grunzweig, A. Hilliard, M. McGovern, and M. F. Andersen, "Near-deterministic preparation of a single atom in an optical microtrap," *Nat. Phys.*, vol. 6, pp. 951–954, Dec. 2010.
- [94] H. A. Pohl, *Dielectrophoresis: The Behavior of Neutral Matter in Nonuniform Electric Fields*. Cambridge: Cambridge Univ. Press, 1978.
- [95] R. Pethig, "Dielectrophoresis: Status of the theory, technology, and applications," *Biomicrofluidics*, vol. 4, pp. 022811–022811–35, June 2010.
- [96] K. Khoshmanesh, S. Nahavandi, S. Baratchi, A. Mitchell, and K. Kalantar-zadeh, "Dielectrophoretic platforms for bio-microfluidic systems," *Biosens. Bioelectron.*, vol. 26, pp. 1800–1814, Jan. 2011.
- [97] A. Ramos, H. Morgan, N. G. Green, and A. Castellanos, "AC electrokinetics—A review of forces in microelectrode structures," *J. Phys. D: Appl. Phys.*, vol. 31, no. 18, pp. 3338–3353, 1998.
- [98] T. B. Jones, "Basic theory of dielectrophoresis and electrorotation," *IEEE Eng. Med. Biol. Mag.*, vol. 22, pp. 33–42, Dec. 2003.
- [99] M. C. Wu, "Optoelectronic tweezers," *Nat. Photon.*, vol. 5, pp. 322–324, June 2011.
- [100] H. Hwang, J. Kim, and J. Park, "Experimental investigation of electrostatic particle interactions in optoelectronic tweezers," *J. Phys. Chem. B*, vol. 112, pp. 9903–9908, Oct. 2011.
- [101] J. K. Valley, A. Jamshidi, A. T. Ohta, H. Hsu, and M. C. Wu, "Operational regimes and physics present in optoelectronic tweezers," *J. Microelectromech. Syst.*, vol. 17, pp. 342–350, Apr. 2008.
- [102] L. V. King, "On the acoustic radiation pressure on spheres," *Proc. Roy. Soc. London. A—Math. Phys. Sci.*, vol. 147, pp. 212–240, Nov. 1934.
- [103] L. P. Gorkov, "On the forces acting on a small particle in an acoustical field in an ideal fluid," Ph.D. dissertation, Soviet Physics Doklady, Kurtchavov Institute, Moscow, Russia, vol. 6, p. 773, Mar. 1962.
- [104] M. Barmatz, "Acoustic radiation potential on a sphere in plane, cylindrical, and spherical standing wave fields," *J. Acoust. Soc. Amer.*, vol. 77, pp. 928–945, 1985.
- [105] C. Liu, L. Lagae, and G. Borghs, "Manipulation of magnetic particles on chip by magnetophoretic actuation and dielectrophoretic levitation," *Appl. Phys. Lett.*, vol. 90, pp. 184109–184112, 2007.
- [106] M. Hagiwara, T. Kawahara, Y. Yamanishi, T. Masuda, L. Feng, and F. Arai, "On-chip magnetically actuated robot with ultrasonic vibration for single cell manipulations," *Lab Chip*, vol. 11, no. 12, pp. 2049–2054, 2011.
- [107] J. Lipfert, M. Wiggin, J. W. Kerssemakers, F. Pedaci, and N. H. Dekker, "Freely orbiting magnetic tweezers to directly monitor changes in the twist of nucleic acids," *Nat. Commun.*, vol. 2, pp. 439–448, 2011.
- [108] L. Arcese, M. Fruchard, and A. Ferreira, "Nonlinear modeling and robust controller-observer for a magnetic microrobot in a fluidic environment using MRI gradients," in *Proc. IEEE/RSJ Int. Conf. Intelligent Robots and Systems, IROS*, 2009, pp. 534–539.
- [109] L. Arcese, A. Cherry, M. Fruchard, and A. Ferreira, "Dynamic behavior investigation for trajectory control of a microrobot in blood vessels," in *Proc. IEEE/RSJ Int. Conf. Intelligent Robots and Systems (IROS)*, 2010, pp. 5774–5779.
- [110] K. Belharet, D. Folio, and A. Ferreira, "MRI-based microrobotic system for the propulsion and navigation of ferromagnetic microcapsules," *Minimal. Invas. Ther. Allied Technol.*, vol. 19, no. 3, pp. 157–169, 2010.
- [111] K. Belharet, D. Folio, and A. Ferreira, "Three-dimensional controlled motion of a microrobot using magnetic gradients," *Adv. Robot.*, vol. 25, no. 8, pp. 1069–1083, 2011.
- [112] R. Probst, J. Lin, A. Komae, A. Nacev, Z. Cummins, and B. Shapiro, "Planar steering of a single ferrofluid drop by optimal minimum power dynamic feedback control of four electromagnets at a distance," *J. Magnet. Magnet. Mater.*, vol. 323, no. 7, pp. 885–896, 2011.
- [113] R. F. Probstein, *Physicochemical Hydrodynamics: An Introduction*, 2nd ed. New York: Wiley, 1994.
- [114] J. Lyklema, H. P. v. Leeuwen, M. v. Vliet, and A. M. Cazabat, *Fundamentals of Interface and Colloid Science*. Academic Press, 2000.
- [115] J. Voldman, "Electrical forces for microscale cell manipulation," *Annu. Rev. Biomed. Eng.*, vol. 8, pp. 425–454, Aug. 2006.
- [116] W. Sutherland, "A dynamical theory of diffusion for non-electrolytes and the molecular mass of albumin," vol. 9, no. 54, pp. 781–785, 1905.
- [117] A. Einstein, "On the movement of small particles suspended in stationary liquids required by the molecular-kinetic theory of heat," *Ann. Phys.*, vol. 17, issue c, pp. 549–560, 1905.
- [118] S. Hardt and F. Schoenfeld, "Microfluidics: Fundamentals and engineering concepts," in *Microfluidic Technologies for Miniaturized Analysis Systems*, S. Hardt and F. Schoenfeld, Eds., Springer, pp. 1–58, 2007.
- [119] W. Sparreboom, A. van den Berg, and J. C. T. Eijkel, "Transport in nanofluidic systems: A review of theory and applications," *New J. Phys.*, vol. 12, pp. 015004–015027, Jan. 2010.
- [120] S. Ghosal, "Fluid mechanics of electroosmotic flow and its effect on band broadening in capillary electrophoresis," *Electrophoresis*, vol. 25, no. 2, pp. 214–228, 2004.
- [121] P. C. Hiemenz and R. Rajagopalan, *Principles of Colloid and Surface Chemistry*, 3rd ed. New York: Marcel Dekker, 1997.
- [122] H. Bruus, *Theoretical Microfluidics*, vol. 18. New York: Oxford Univ. Press, 2008.
- [123] H. Chang and L. Y. Yeo, *Electrokinetically Driven Microfluidics and Nanofluidics*. Cambridge, New York: Cambridge Univ. Press, 2010.
- [124] H. Bruus, A. Brask, and J. P. Kutter, "Nanofluidic components for electrokinetic micropumps," *Adv. Nat. Sci.*, vol. 5, no. 4, pp. 423–430, 2004.
- [125] A. Sale and W. Hamilton, "Effects of high electric fields on microorganisms. I. Killing of bacteria and yeasts," *Biochim. Biophys. Acta*, vol. 148, pp. 781–788, Dec. 1967.
- [126] J. Weaver and R. Astumian, "The response of living cells to very weak electric fields: The thermal noise limit," *Science*, vol. 247, pp. 459–462, Jan. 1990.
- [127] J. Teissie, N. Eynard, B. Gabriel, and M. P. Rols, "Electropermeabilization of cell membranes," *Adv. Drug Deliv. Rev.*, vol. 35, pp. 3–19, Jan. 1999.
- [128] R. C. Lee, "Cell injury by electric forces," *Ann. New York Acad. Sci.*, vol. 1066, no. 1, pp. 85–91, 2006.
- [129] S. V. Chaudhary, "Precise steering of particles in electroosmotically actuated microfluidic devices," Ph.D. dissertation, Univ. Maryland, College Park, MD, 2010.
- [130] G. E. Karniadakis and A. Beskok, *Micro Flows: Fundamentals and Simulation*. New York: Springer-Verlag, 2001.
- [131] T. Zhang and S. E. Lyshevsky, *Microelectrofluidic Systems: Modeling and Simulation*. Boca Raton, FL: CRC Press, 2002.
- [132] B. Kirby, *Micro- and Nanoscale Fluid Mechanics: Transport in Microfluidic Devices*. New York: Cambridge Univ. Press, 2010.
- [133] J. O. Wilkes, B. J. Kirby, S. G. Birmingham, and C. Y. Cheng, *Fluid Mechanics for Chemical Engineers with Microfluidics and CFD*. Englewood Cliffs, NJ: Prentice Hall, 2006.
- [134] L. Pauling, *General Chemistry*. New York: Dover, 1970.
- [135] G. Karniadakis, A. Beskok, and N. R. Aluru, *Microflows and Nanoflows: Fundamentals and Simulation*. New York: Springer-Verlag, 2005.
- [136] R. L. Panton, *Incompressible Flow*, 2nd ed. New York: Wiley, 1996.
- [137] T. Zhou, A. Liu, F. He, and X. Xia, "Time-dependent starting profile of velocity upon application of external electrical potential in electroosmotic

- driven microchannels," *Colloids Surf. A: Physicochem. Eng. Aspects*, vol. 277, no. 1–3, pp. 136–144, 2006.
- [138] S. Walker and B. Shapiro, "Modeling the fluid dynamics of electro-wetting on dielectric (EWOD)," *J. Microelectromech. Syst.*, vol. 15, no. 4, pp. 986–1000, 2006.
- [139] G. K. Batchelor, *An Introduction to Fluid Dynamics*. Cambridge: Cambridge Univ. Press, 1967.
- [140] A. A. Darhuber and S. M. Troian, "Principles of microfluidic actuation by modulation of surface stresses," *Annu. Rev. Fluid Mech.*, vol. 37, pp. 425–455, Jan. 2005.
- [141] F. F. Reuss, "Sur un nouvel effet de l'electricite galvanique," *Mem. Soc. Imp. Natur. Moscou*, vol. 2, pp. 327–337, 1809.
- [142] V. Pretorius, B. Hopkins, and J. Schieke, "Electro-osmosis: A new concept for high-speed liquid chromatography," *J. Chromatogr. A*, vol. 99, pp. 23–30, Nov. 6, 1974.
- [143] O. Soderman and B. Jonsson, "Electro-osmosis: Velocity profiles in different geometries with both temporal and spatial resolution," *J. Chem. Phys.*, vol. 105, pp. 10300–10311, Dec. 1996.
- [144] P. J. Resto, B. J. Mogen, E. Berthier, and J. C. Williams, "An automated microdroplet passive pumping platform for high-speed and packeted microfluidic flow applications," *Lab Chip*, vol. 10, no. 1, pp. 23–26, 2010.
- [145] F. Mugele and J. C. Baret, "Electrowetting: From basics to applications," *J. Phys.: Condens. Matter*, vol. 17, no. 28, pp. R705–R774, 2005.
- [146] P. S. Glockner and G. F. Naterer, "Thermocapillary control of microfluidic transport with a stationary cyclic heat source," *J. Micromech. Microeng.*, vol. 15, no. 12, pp. 2216–2229, 2005.
- [147] G. M. Walker and D. J. Beebe, "An evaporation-based microfluidic sample concentration method," *Lab Chip*, vol. 2, no. 2, pp. 57–61, 2002.
- [148] G. Lippmann, "Relation entre les phenomenes electriques et capillaires," *Ann. Chim. Phys.*, vol. 5, no. 5, pp. 494–549, 1875.
- [149] M. Vallet, B. Berge, and L. Vovelle, "Electrowetting of water and aqueous solutions on poly(ethyleneterephthalate) insulating films," *Eur. Phys. J.*, vol. 11, no. 12, pp. 583–591, 1996.
- [150] J. Lee and C. J. Kim, "Surface tension driven microactuation based on continuous electro-wetting (CEW)," *J. Microelectromech. Syst.*, vol. 9, no. 2, pp. 171–180, 2000.
- [151] M. G. Pollack and A. D. Shenderov, "Electrowetting-based actuation of liquid droplets for microfluidic applications," *Appl. Phys. Lett.*, vol. 77, no. 11, pp. 1725–1727, 2000.
- [152] S. K. Cho and C. J. Kim, "Splitting a liquid droplet for electro-wetting-based microfluidics," in *Proc. Int. Mechanical Engineering Congr. Exposition, IMECE2001/MEMS-23831*, New York, 2001, pp. 23,831–23,838.
- [153] K. H. Kang, "How electrostatic fields change contact angle in electro-wetting," *Langmuir*, vol. 18, no. 26, pp. 10318–10322, 2002.
- [154] J. Lee, H. Moon, J. Fowler, T. Schoellhammer, and C. J. Kim, "Electrowetting and electro-wetting-on-dielectric for microscale liquid handling," *Sensor Actuat. A Phys.*, vol. 95, no. 2–3, pp. 259–268, 2002.
- [155] S. K. Cho and C. J. Kim, "Creating, transporting, cutting, and merging liquid droplets by electro-wetting-based actuation for digital microfluidic circuits," *J. Microelectromech. Syst.*, vol. 12, no. 1, pp. 70–80, 2003.
- [156] C. J. Kim, "Micropumping by electro-wetting," in *Proc. Int. Mechanical Engineering Congr. Exposition, IMECE2001/HTD-24200*, New York, 2001, pp. 24,200–24,204.
- [157] M. G. Pollack, A. D. Shenderov, and R. B. Fair, "Electrowetting-based actuation of droplets for integrated microfluidics," *Lab Chip*, vol. 2, no. 2, pp. 96–101, 2002.
- [158] P. Paik, V. K. Pamula, and R. B. Fair, "Rapid droplet mixers for digital microfluidic systems," *Lab Chip*, vol. 3, pp. 253–259, Nov. 2003.
- [159] V. Srinivasan and R. Fair, "A digital microfluidic biosensor for multianalyte detection," in *Proc. IEEE 16th Annu. Int. Conf. Micro Electro Mechanical Systems*, 2003, pp. 327–330.
- [160] S. K. Chung, K. Rhee, and S. K. Cho, "Bubble actuation by electro-wetting-on-dielectric (EWOD) and its applications: A review," *Int. J. Precis. Eng. Manufact.*, vol. 11, pp. 991–1006, Dec. 2010.
- [161] B. Berge and J. Peseux, "Variable focal lens controlled by an external voltage: An application of electro-wetting," *Eur. Phys. J.*, vol. 3, no. 2, pp. 159–163, 2000.
- [162] B. Berge, "Liquid lens technology: Principle of electro-wetting based lenses and applications to imaging," *Micro. Electro. Mech. Syst.*, 18th IEEE Int. Conf. on MEMS 2005, pp. 227–230, Jan. 2005.
- [163] R. A. Hayes and B. J. Feenstra, "Video-speed electronic paper based on electro-wetting," *Nature*, vol. 425, no. 6956, pp. 383–385, 2003.
- [164] T. Roques-Carmes, R. A. Hayes, B. J. Feenstra, and L. J. M. Schlangen, "Liquid behavior inside a reflective display pixel based on electro-wetting," *J. Appl. Phys.*, vol. 95, no. 8, pp. 4389–4396, 2004.
- [165] T. Roques-Carmes, R. A. Hayes, and L. J. M. Schlangen, "A physical model describing the electro-optic behavior of switchable optical elements based on electro-wetting," *J. Appl. Phys.*, vol. 96, no. 11, pp. 6267–6271, 2004.
- [166] T. Roques-Carmes, S. Palmier, R. A. Hayes, and L. J. M. Schlangen, "The effect of the oil/water interfacial tension on electro-wetting driven fluid motion," *Colloids Surf. A Physicochem. Eng. Aspects*, vol. 267, no. 1–3, pp. 56–63, 2005.
- [167] B. Shapiro, H. Moon, R. Garrell, and C. J. Kim, "Equilibrium behavior of sessile drops under surface tension, applied external fields, and material variations," *J. Appl. Phys.*, vol. 93, no. 9, pp. 5794–5812, 2003.
- [168] R. G. Cox, "The dynamics of the spreading of liquids on a solid-surface. 1. Viscous-flow," *J. Fluid Mech.*, vol. 168, pp. 169–194, July 1986.
- [169] R. G. Cox, "The dynamics of the spreading of liquids on a solid-surface. 2. Surfactants," *J. Fluid Mech.*, vol. 168, pp. 195–220, July 1986.
- [170] J. A. Marsh, S. Garoff, and E. B. Dussan, "Dynamic contact angles and hydrodynamics near a moving contact line," *Phys. Rev. Lett.*, vol. 70, no. 18, pp. 2778–2781, 1993.
- [171] H. J. Verheijen and M. W. J. Prins, "Reversible electro-wetting and trapping of charge: Model and experiments," *Langmuir*, vol. 15, no. 20, pp. 6616–6620, 1999.
- [172] M. Vallet, M. Vallade, and B. Berge, "Limiting phenomena for the spreading of water on polymer films by electro-wetting," *Eur. Phys. J.*, vol. 11, no. 4, pp. 583–591, 1999.
- [173] V. Peykov, A. Quinn, and J. Ralston, "Electro-wetting: A model for contact-angle saturation," *Colloid Polymer Sci.*, vol. 278, no. 8, pp. 789–793, 2000.
- [174] R. Digilov, "Charge-induced modification of contact angle: the secondary electrocapillary effect," *Langmuir*, vol. 16, no. 16, pp. 6719–6723, 2000.
- [175] H. Ren, R. B. Fair, M. G. Pollack, and E. J. Shaughnessy, "Dynamics of electro-wetting droplet transport," *Sens. Actuat. B Chem.*, vol. 87, no. 1, pp. 201–206, 2002.
- [176] T. B. Jones, "On the relationship of dielectrophoresis and electro-wetting," *Langmuir*, vol. 18, no. 11, pp. 4437–4443, 2002.
- [177] T. B. Jones, J. D. Fowler, Y. S. Chang, and C. J. Kim, "Frequency-based relationship of electro-wetting and dielectrophoretic liquid microactuation," *Langmuir*, vol. 19, no. 18, pp. 7646–7651, 2003.
- [178] H.-W. Lu, K. Glasner, A. L. Bertozzi, and C.-J. Kim, "A diffuse-interface model for electro-wetting drops in a Hele-Shaw cell," *J. Fluid Mech.*, vol. 590, pp. 411–435, 2007.
- [179] K. L. Wang and T. B. Jones, "Electro-wetting dynamics of microfluidic actuation," *Langmuir*, vol. 21, no. 9, pp. 4211–4217, 2005.
- [180] A. Dolatabadi and K. Mohseni, "Behavior of a moving droplet under electro-wetting actuation in microchannel," in *Proc. ICMENS*, Banff, AB, Canada, 2005, pp. 95–96.
- [181] T. D. Blake, "The physics of moving wetting lines," *J. Colloid Interface Sci.*, vol. 299, no. 1, pp. 1–13, 2006.
- [182] J. L. Lin, G. B. Lee, Y. H. Chang, and K. Y. Lien, "Model description of contact angles in electro-wetting on dielectric layers," *Langmuir*, vol. 22, no. 1, pp. 484–489, 2006.
- [183] S. W. Walker, B. Shapiro, and R. H. Nochetto, "Electro-wetting with contact line pinning: Computational modeling and comparisons with experiments," *Phys. Fluids*, vol. 23, no. 10, pp. 102103–102119, 2009.
- [184] H. Hu and R. G. Larson, "Analysis of the effects of marangoni stresses on the microflow in an evaporating sessile droplet," *Langmuir*, vol. 21, no. 9, pp. 3972–3980, 2005.
- [185] A. S. Basu and Y. B. Gianchandani, "Virtual microfluidic traps, filters, channels and pumps using marangoni flows," *J. Micromech. Microeng.*, vol. 18, pp. 115031–115042, Nov. 2008.

- [186] Y. Popov, "Singularities, universality, and scaling in evaporative deposition patterns," Ph.D. dissertation, Dept. of Physics., Univ. Chicago, Dec. 2003.
- [187] S. Walker and B. Shapiro, "A control method for steering individual particles inside liquid droplets actuated by electrowetting," *Lab Chip*, vol. 12, no. 1, pp. 1404–1407, 2005.
- [188] P. Holmes, *Turbulence, Coherent Structures, Dynamical Systems and Symmetry*, 1st paperback edition. Cambridge: Cambridge Univ. Press, 1998.
- [189] B. R. Noack, K. Afanasiev, M. Morzynski, G. Tadmor, and F. Thiele, "A hierarchy of low-dimensional models for the transient and post-transient cylinder wake," *J. Fluid Mech.*, vol. 497, no. 1, pp. 335–363, 2003.
- [190] A. C. Antoulas, *Approximation of Large-Scale Dynamical Systems* (Advances in Design and Control, vol. 6). Society for Industrial Mathematics, Cambridge University Press, 2005.
- [191] C. W. Rowley, "Model reduction for fluids, using balanced proper orthogonal decomposition," *Int. J. Bifurcat. Chaos Appl. Sci. Eng.*, vol. 15, no. 3, pp. 997–1014, 2005.
- [192] D. Vasilyev, M. Rewienski, and J. White, "Macromodel generation for BioMEMS components using a stabilized balanced truncation plus trajectory piecewise-linear approach," *IEEE Trans. Comput.-Aided Design Integr. Circuits Syst.*, vol. 25, pp. 285–293, Feb. 2006.
- [193] Y. J. Yang and C. Kuo, "Generating scalable and modular macromodels for microchannels using the Galerkin-based technique," *IEEE Trans. on Comp.-Aided Design of Integ. Cir. and Syst.*, vol. 27, pp. 1545–1554, Sept. 2008.
- [194] H. Antil, M. Heinkenschloss, R. H. W. Hoppe, C. Linsenmann, and A. Wixforth. (2010, Nov. 11). Reduced order modeling based shape optimization of surface acoustic wave driven microfluidic chips. *Mathematics and Computers in Simulation*. [Online]. Available: <http://www.sciencedirect.com/science/article/pii/S0378475410003496>
- [195] R. Brown, "A brief account of microscopical observations made in the months of June, July and August 1827 on the particles contained in the pollen of plants," *Phil. Mag.*, vol. 4, no. 1828, pp. 161–173.
- [196] D. T. Gillespie, "The mathematics of Brownian motion and Johnson noise," *Amer. J. Phys.*, vol. 64, no. 3, pp. 225–239, 1996.
- [197] S. Chaudhary and B. Shapiro, "Arbitrary steering of multiple particles at once in an electroosmotically driven microfluidic system," *IEEE Trans. Contr. Syst. Technol.*, vol. 14, no. 4, pp. 669–680, 2006.
- [198] F. Perrin, "Brownian movement of an ellipsoid. I. Dielectric dispersion of an ellipsoidal molecule," *J. Phys. Rad.*, vol. 5, no. 10, pp. 497–511, 1934.
- [199] F. Perrin, "Brownian movement of ellipsoids. II. Free rotation and depolarization of fluorescence. Translation and diffusion of ellipsoidal molecules," *J. Phys. Rad.*, vol. 7, no. 1, pp. 1–11, 1936.
- [200] J. T. Padding and W. J. Briels, "Translational and rotational friction on a colloidal rod near a wall," *J. Chem. Phys.*, vol. 132, no. 5, pp. 054511–054519, 2010.
- [201] M. Rubinstein, *Polymer Physics*. Oxford New York: Oxford Univ. Press, 2003.
- [202] E. S. G. Shaqfeh, "The dynamics of single-molecule DNA in flow," *J. Non-Newton. Fluid Mech.*, vol. 130, pp. 1–28, Oct. 2005.
- [203] J. Maarel, *Introduction to Biopolymer Physics*. Hackensack NJ: World Scientific, 2007.
- [204] C. C. Hsieh and P. S. Doyle, "Studying confined polymers using single-molecule DNA experiments," *Korea-Australia Rheol. J.*, vol. 20, no. 3, pp. 127–142, 2008.
- [205] Z. Wang, M. J. Kim, and G. Rosen, "Validating models of bacterial chemotaxis by simulating the random motility coefficient," *Bioinfo. and Bioeng.*, 8th IEEE Int. Conf. on BIBI 2008, Athens, 8–10 Oct. 2008, pp. 1–5.
- [206] E. Lauga, W. R. DiLuzio, G. M. Whitesides, and H. A. Stone, "Swimming in circles: Motion of bacteria near solid boundaries," *Biophys. J.*, vol. 90, no. 2, pp. 400–412, 2006.
- [207] S. L. Neale, M. Mazilu, J. I. B. Wilson, K. Dholakia, and T. F. Krauss, "The resolution of optical traps created by light induced dielectrophoresis (LIDEP)," *Opt. Express*, vol. 15, pp. 12619–12626, Oct. 2007.
- [208] J. Lipfert, X. Hao, and N. H. Dekker, "Quantitative modeling and optimization of magnetic tweezers," *Biophys. J.*, vol. 96, pp. 5040–5049, June 2009.
- [209] N. A. Patankar and H. H. Hu, "Numerical simulation of electroosmotic flow," *Anal. Chem.*, vol. 70, no. 9, pp. 1870–1881, 1998.
- [210] D. Yan, N. Nguyen, C. Yang, and X. Huang, "Visualizing the transient electroosmotic flow and measuring the zeta potential of microchannels with a micro-PIV technique," *J. Chem. Phys.*, vol. 124, no. 2, pp. 021103–021107, 2006.
- [211] R. P. Feynman, R. B. Leighton, and M. Sands, *The Feynman Lectures on Physics*. Reading, MA: Addison-Wesley, 1964.
- [212] K. Makino and H. Ohshima, "Soft particle analysis of electrokinetics of biological cells and their model systems," *Sci. Technol. Adv. Mater.*, vol. 12, no. 2, pp. 023001–023012, 2011.
- [213] R. G. Ehl and A. J. Ihde, "Faraday's electrochemical laws and the determination of equivalent weights," *J. Chem. Educ.*, vol. 31, pp. 226–232, May 1954.
- [214] I. Gitlin, A. D. Stroock, G. M. Whitesides, and A. Ajdari, "Pumping based on transverse electrokinetic effects," *Appl. Phys. Lett.*, vol. 83, no. 7, pp. 1486–1489, 2003.
- [215] R. Probst and B. Shapiro, "Three-dimensional electrokinetic tweezing: Device design, modeling, and control algorithms," *J. Micromech. Microeng.*, vol. 21, part 027004, Feb. 2011.
- [216] Y. Takamura, H. Onoda, H. Inokuchi, S. Adachi, A. Oki, and Y. Horiike, "Low-voltage electroosmosis pump for stand-alone microfluidics devices," *Electrophoresis*, vol. 24, no. 1–2, pp. 185–192, 2003.
- [217] A. Persat, R. D. Chambers, and J. G. Santiago, "Basic principles of electrolyte chemistry for microfluidic electrokinetics. Part I: Acid-base equilibria and pH buffers," *Lab Chip*, vol. 9, pp. 2437–2453, 2009.
- [218] P. G. Erlandsson and N. D. Robinson, "Electrolysis reducing electrodes for electrokinetic devices," *Electrophoresis*, vol. 32, pp. 784–790, Mar. 2011.
- [219] K. Pantel, C. Alix-Panabieres, and S. Riethdorf, "Cancer micrometastases," *Nat. Rev. Clin. Oncol.*, vol. 6, pp. 339–351, June 2009.
- [220] Y. Huesemann, J. B. Geigl, F. Schubert, P. Musiani, M. Meyer, E. Burghart, G. Forni, R. Eils, T. Fehm, G. Riethmueller, and C. A. Klein, "Systemic spread is an early step in breast cancer," *Cancer Cell*, vol. 13, pp. 58–68, Jan. 2008.
- [221] G. N. Naumov, I. C. MacDonald, P. M. Weinmeister, N. Kerkvliet, K. V. Nadkarni, S. M. Wilson, V. L. Morris, A. C. Groom, and A. F. Chambers, "Persistence of solitary mammary carcinoma cells in a secondary site: A possible contributor to dormancy," *Cancer Res.*, vol. 62, pp. 2162–2168, Apr. 2002.
- [222] A. F. Chambers, A. C. Groom, and I. C. MacDonald, "Dissemination and growth of cancer cells in metastatic sites," *Nat. Rev. Cancer*, vol. 2, no. 8, pp. 563–571, 2002.
- [223] G. N. Naumov, J. L. Townson, I. C. MacDonald, S. M. Wilson, V. H. C. Bramwell, A. C. Groom, and A. F. Chambers, "Ineffectiveness of doxorubicin treatment on solitary dormant mammary carcinoma cells or late-developing metastases," *Breast Cancer Res. Treat.*, vol. 82, pp. 199–206, Dec. 2003.
- [224] G. Li, H. Xie, H. Ning, D. Citrin, J. Capala, R. Maass-Moreno, P. Guion, B. Arora, N. Coleman, K. Camphausen, and R. W. Miller, "Accuracy of 3D volumetric image registration based on CT, MR and PET/CT phantom experiments," *J. Appl. Clin. Med. Phys./Amer. College of Med. Phys.*, vol. 9, no. 4, pp. 2781–2800, 2008.
- [225] C. A. Klein, T. J. F. Blankenstein, O. Schmidt-Kittler, M. Petronio, B. Polzer, N. H. Stoecklein, and G. Riethmueller, "Genetic heterogeneity of single disseminated tumour cells in minimal residual cancer," *Lancet*, vol. 360, pp. 683–689, Aug. 2002.
- [226] S. Riethdorf, H. Wikman, and K. Pantel, "Review: Biological relevance of disseminated tumor cells in cancer patients," *Int. J. Cancer*, vol. 123, pp. 1991–2006, Nov. 2008.
- [227] H. Yamaguchi and J. Condeelis, "Regulation of the actin cytoskeleton in cancer cell migration and invasion," *Biochim. Biophys. Acta*, vol. 1773, pp. 642–652, May 2007.
- [228] H. Yamaguchi, J. Wyckoff, and J. Condeelis, "Cell migration in tumors," *Curr. Opin. Cell Biol.*, vol. 17, pp. 559–564, Oct. 2005.
- [229] R. A. Whipple, E. M. Balzer, E. H. Cho, M. A. Matrone, J. R. Yoon, and S. S. Martin, "Vimentin filaments support extension of tubulin-based microtentacles in detached breast tumor cells," *Cancer Res.*, vol. 68, pp. 5678–5688, July 2008.
- [230] E. M. Balzer, R. A. Whipple, K. Thompson, A. E. Boggs, J. Slovic, E. H. Cho, M. A. Matrone, T. Yoneda, S. C. Mueller, and S. S. Martin, "c-Src differentially regulates the functions of microtentacles and invadopodia," *Oncogene*, vol. 29, pp. 6402–6408, Dec. 2010.
- [231] M. A. Matrone, R. A. Whipple, K. Thompson, E. H. Cho, M. I. Vitolo, E. M. Balzer, J. R. Yoon, O. B. Ioffe, K. C. Tuttle, M. Tan, and S. S. Martin, "Metastatic breast tumors express increased tau, which promotes

- microtentacle formation and the reattachment of detached breast tumor cells," *Oncogene*, vol. 29, pp. 3217–3227, June 2010.
- [232] M. A. Matrone, R. A. Whipple, E. M. Balzer, and S. S. Martin, "Microtentacles tip the balance of cytoskeletal forces in circulating tumor cells," *Cancer Res.*, vol. 70, pp. 7737–7741, Oct. 2010.
- [233] C. P. Brangwynne, F. C. MacKintosh, S. Kumar, N. A. Geisse, J. Talbot, L. Mahadevan, K. K. Parker, D. E. Ingber, and D. A. Weitz, "Microtubules can bear enhanced compressive loads in living cells because of lateral reinforcement," *J. Cell Biol.*, vol. 173, pp. 733–741, June 2006.
- [234] S. Even-Ram, A. D. Doyle, M. A. Conti, K. Matsumoto, R. S. Adelstein, and K. M. Yamada, "Myosin IIA regulates cell motility and actomyosin-microtubule crosstalk," *Nat. Cell Biol.*, vol. 9, pp. 299–309, Mar. 2007.
- [235] R. A. Whipple, A. M. Cheung, and S. S. Martin, "Detyrosinated microtubule protrusions in suspended mammary epithelial cells promote reattachment," *Exp. Cell Res.*, vol. 313, pp. 1326–1336, Apr. 2007.
- [236] O. Camara, M. Rengsberger, A. Egbe, A. Koch, M. Gajda, U. Hammer, C. Joerke, C. Rabenstein, M. Untch, and K. Pachmann, "The relevance of circulating epithelial tumor cells (CETC) for therapy monitoring during neoadjuvant (primary systemic) chemotherapy in breast cancer," *Ann. Oncol.: Official J. Eur. Soc. Med. Oncol./ESMO*, vol. 18, pp. 1484–1492, Sept. 2007.
- [237] K. Pachmann, O. Camara, A. Kavallaris, S. Krauspe, N. Malarski, M. Gajda, T. Kröll, C. Joerke, U. Hammer, A. Altendorf-Hofmann, C. Rabenstein, U. Pachmann, I. Runnebaum, and K. Hoeffken, "Monitoring the response of circulating epithelial tumor cells to adjuvant chemotherapy in breast cancer allows detection of patients at risk of early relapse," *J. Clin. Oncol.: Official J. Amer. Soc. Clin. Oncol.*, vol. 26, pp. 1208–1215, Mar. 2008.
- [238] E. M. Balzer, R. A. Whipple, E. H. Cho, M. A. Matrone, and S. S. Martin, "Antimitotic chemotherapeutics promote adhesive responses in detached and circulating tumor cells," *Breast Cancer Res. Treat.*, vol. 121, pp. 65–78, May 2010.
- [239] C. Alix-Panabières, V. Müller, and K. Pantel, "Current status in human breast cancer micrometastasis," *Curr. Opin. Oncol.*, vol. 19, pp. 558–563, Nov. 2007.
- [240] T. Fehm, V. Mueller, C. Alix-Panabieres, and K. Pantel, "Micrometastatic spread in breast cancer: Detection, molecular characterization and clinical relevance," *Breast Cancer Res.*, vol. 10 suppl. 1, pp. S1–S10, 2008.
- [241] B. Willipinski-Stapelfeldt, S. Riethdorf, V. Assmann, U. Woelfle, T. Rau, G. Sauter, J. Heukeshoven, and K. Pantel, "Changes in cytoskeletal protein composition indicative of an epithelial-mesenchymal transition in human micrometastatic and primary breast carcinoma cells," *Clin. Cancer Res.: Official J. Amer. Assoc. Cancer Res.*, vol. 11, pp. 8006–8014, Nov. 2005.
- [242] S. Nagrath, L. V. Sequist, S. Maheswaran, D. W. Bell, D. Irimia, L. Ulkus, M. R. Smith, E. L. Kwak, S. Digumarthy, A. Muzikansky, P. Ryan, U. J. Balis, R. G. Tompkins, D. A. Haber, and M. Toner, "Isolation of rare circulating tumour cells in cancer patients by microchip technology," *Nature*, vol. 450, no. 20, pp. 1235–1239, 2007.
- [243] B. Aktas, M. Tewes, T. Fehm, S. Hauch, R. Kimmig, and S. Kasimir-Bauer, "Stem cell and epithelial-mesenchymal transition markers are frequently overexpressed in circulating tumor cells of metastatic breast cancer patients," *Breast Cancer Res.*, vol. 11, no. 4, pp. R46–R55, 2009.
- [244] C. G. Rao, D. Chianese, G. V. Doyle, M. C. Miller, T. Russell, J. Sanders, A. Renouard, and L. W. M. M. Terstappen, "Expression of epithelial cell adhesion molecule in carcinoma cells present in blood and primary and metastatic tumors," *Int. J. Oncol.*, vol. 27, pp. 49–57, July 2005.
- [245] A. A. Adams, P. I. Okagbare, J. Feng, M. L. Hupert, D. Patterson, J. Goertert, R. L. McCarley, D. Nikitopoulos, M. C. Murphy, and S. A. Soper, "Highly efficient circulating tumor cell isolation from whole blood and label-free enumeration using polymer-based microfluidics with an integrated conductivity sensor," *J. Amer. Chem. Soc.*, vol. 130, pp. 8633–8641, July 2008.
- [246] S. L. Stott, C. Hsu, D. I. Tsukrov, M. Yu, D. T. Miyamoto, B. A. Waltman, S. M. Rothenberg, A. M. Shah, M. E. Smas, G. K. Korir, J. Floyd, Frederick P. A. J. Gilman, J. B. Lord, D. Winokur, S. Springer, D. Irimia, S. Nagrath, L. V. Sequist, R. J. Lee, K. J. Isselbacher, S. Maheswaran, D. A. Haber, and M. Toner, "Isolation of circulating tumor cells using a microvortex-generating herringbone-chip," *Proc. Nat. Acad. Sci. USA*, vol. 107, pp. 18392–18397, Oct. 2010.
- [247] S. Zheng, H. K. Lin, B. Lu, A. Williams, R. Datar, R. J. Cote, and Y. Tai, "3D microfilter device for viable circulating tumor cell (CTC) enrichment from blood," *Biomed. Microdev.*, vol. 13, pp. 203–213, Feb. 2011.
- [248] H. K. Lin, S. Zheng, A. J. Williams, M. Balic, S. Groshen, H. I. Scher, M. Fleisher, W. Stadler, R. H. Datar, Y. Tai, and R. J. Cote, "Portable filter-based microdevice for detection and characterization of circulating tumor cells," *Clin. Cancer Res.: Official J. Amer. Assoc. Cancer Res.*, vol. 16, pp. 5011–5018, Oct. 2010.
- [249] M. Paulitschke, J. Mikita, D. Lerche, and W. Meier, "Elastic properties of passive leukemic white blood cells," *Int. J. Microcirculation, Clinical and Experimental*, vol. 10, pp. 67–73, Feb. 1991.
- [250] Y. Chu, W. A. Thomas, O. Eder, F. Pincet, E. Perez, J. P. Thiery, and S. Dufour, "Force measurements in e-cadherin-mediated cell doublets reveal rapid adhesion strengthened by actin cytoskeleton remodeling through rac and cdc42," *J. Cell Biol.*, vol. 167, pp. 1183–1194, Dec. 2004.
- [251] J. Guck, S. Schinkinger, B. Lincoln, F. Wottawah, S. Ebert, M. Romeyke, D. Lenz, H. M. Erickson, R. Ananthkrishnan, D. Mitchell, J. Kaes, S. Ulvick, and C. Bilby, "Optical deformability as an inherent cell marker for testing malignant transformation and metastatic competence," *Biophys. J.*, vol. 88, pp. 3689–3698, May 2005.
- [252] T. W. Remmerbach, F. Wottawah, J. Dietrich, B. Lincoln, C. Wittekind, and J. Guck, "Oral cancer diagnosis by mechanical phenotyping," *Cancer Res.*, vol. 69, pp. 1728–1732, Mar. 2009.
- [253] F. Wottawah, S. Schinkinger, B. Lincoln, R. Ananthkrishnan, M. Romeyke, J. Guck, and J. Kaes, "Optical rheology of biological cells," *Phys. Rev. Lett.*, vol. 94, part 098103, Mar. 2005.
- [254] A. B. Al-Mehdi, K. Tozawa, A. B. Fisher, L. Shientag, A. Lee, and R. J. Muschel, "Intravascular origin of metastasis from the proliferation of endothelium-attached tumor cells: A new model for metastasis," *Nat. Med.*, vol. 6, pp. 100–102, Jan. 2000.
- [255] J. R. Yoon, R. A. Whipple, E. M. Balzer, E. H. Cho, M. A. Matrone, M. Peckham, and S. S. Martin, "Local anesthetics inhibit kinesin motility and microtentacle protrusions in human epithelial and breast tumor cells," *Breast Cancer Res. Treat.*, vol. 129, pp. 691–701, Oct. 2011.
- [256] R. A. Whipple, M. A. Matrone, E. H. Cho, E. M. Balzer, M. I. Vitolo, J. R. Yoon, O. B. Ioffe, K. C. Tuttle, J. Yang, and S. S. Martin, "Epithelial-to-mesenchymal transition promotes tubulin detyrosination and microtentacles that enhance endothelial engagement," *Cancer Res.*, vol. 70, pp. 8127–8137, Oct. 2010.
- [257] T. B. Jones, "Influence of scale on electrostatic forces and torques in AC particulate electrokinetics," *IEE Proc. Nanobiotechnol.*, vol. 150, pp. 39–46, Nov. 2003.
- [258] J. Lim, C. Lanni, E. R. Everts, F. Lanni, R. D. Tilton, and S. A. Majetich, "Magnetophoresis of nanoparticles," *ACS Nano*, vol. 5, no. 1, pp. 217–226, 2010.
- [259] A. Badolato, K. Hennessy, M. Atature, J. Dreiser, E. Hu, P. M. Petroff, and A. Imamoglu, "Deterministic coupling of single quantum dots to single nanocavity modes," *Science*, vol. 308, no. 5725, pp. 1158–1161, May 2005.
- [260] D. Englund, A. Faraon, I. Fushman, N. Stoltz, P. Petroff, and J. Vuckovic, "Controlling cavity reflectivity with a single quantum dot," *Nature*, vol. 450, no. 7171, pp. 857–861, Dec. 2007.
- [261] K. Hennessy, A. Badolato, M. Winger, D. Gerace, M. Atature, S. Gulde, S. Falt, E. L. Hu, and A. Imamoglu, "Quantum nature of a strongly coupled single quantum dot-cavity system," *Nature*, vol. 445, no. 7130, pp. 896–899, Feb. 2007.
- [262] A. V. Akimov, A. Mukherjee, C. L. Yu, D. E. Chang, A. S. Zibrov, P. R. Hemmer, H. Park, and M. D. Lukin, "Generation of single optical plasmons in metallic nanowires coupled to quantum dots," *Nature*, vol. 450, no. 7168, pp. 402–406, Nov. 15, 2007.
- [263] D. E. Chang, A. S. Sorensen, E. A. Demler, and M. D. Lukin, "A single-photon transistor using nanoscale surface plasmons," *Nat. Phys.*, vol. 3, no. 11, pp. 807–812, Aug. 2007.
- [264] M. Barth, J. Kouba, J. Stingl, B. Loechel, and O. Benson, "Modification of visible spontaneous emission with silicon nitride photonic crystal nanocavities," *Opt. Express*, vol. 15, no. 25, pp. 17231–17240, 2007.
- [265] R. E. Thompson, D. R. Larson, and W. W. Webb, "Precise nanometer localization analysis for individual fluorescent probes," *Biophys. J.*, vol. 82, no. 5, pp. 2775–2783, 2002.
- [266] X. Peng, L. Manna, W. Yang, J. Wickham, E. Scher, A. Kadvanich, and A. P. Alivisatos, "Shape control of CdSe nanocrystals," *Nature*, vol. 404, pp. 59–61, 2000.
- [267] A. Nacev, A. Komae, A. Sarwar, R. Probst, S. Kim, M. Emmert-Buck, and B. Shapiro, "Towards control of magnetic fluids in patients," *IEEE Cont. Syst. Mag.*, to be published.